ISTITUTO NAZIONALE DI FISICA NUCLEARE

Sezione di Padova

INFN/AE-88/10
26 Settembre 1988

A. Bettini:

**Probing the Standard Model at the SPS Collider.
Experimental Results from UA1**

Servizio Documentazione
dei Laboratori Nazionali di Frascati

INFN - Istituto Nazionale di Fisica Nucleare
Sezione di Padova

INFN/AE-88/10
26 Settembre 1988

Probing the Standard Model at the SPS Collider. Experimental Results from UA1

A. Bettini
Dipartimento di Fisica and INFN, Sezione di Padova (Italy)

1. INTRODUCTION

In these lectures a review of the experimental results which have been obtained by the UA1 experiment at the CERN $p\bar{p}$ collider is presented. When relevant, results from the parallel UA2 experiment are quoted for comparison. Both experiments collected data in a series of data taking periods between 1982 and 1985 at centre of mass energies $\sqrt{s} = 546$ GeV and, mostly, at $\sqrt{s} = 630$ GeV. The total integrated luminosity is between 0.7 and 0.8 events per picobarn (pb^{-1}).

The experimental results will be compared with the predictions of the Electroweak theory in Sections 4.2 - 4.6 and 5.2 and of the Quantum Cromo-Dynamics in Chapter 5. The observation of the W in all the three expected leptonic channels ($W \to e\nu_e$, $W \to \mu\nu_\mu$, $W \to \tau\nu_\tau$) and of the Z^0 in both the electron and muon channels ($Z^0 \to e^+ e^-$, $Z^0 \to \mu^+ \mu^-$) will be reviewed as well as the measurements of their masses and decay properties. Complete agreement will be found with the predictions of the Electroweak theory. The production properties of the intermediate vector bosons (production cross sections and differential cross sections) will be found in agreement with the predictions of QCD.

As discussed in Section 5.3 and Chapters 7 and 8, the data put significant limits on extensions and/or modifications of the standard model; in particular limits are obtained on the masses of the top quark and of the charged lepton of a possible fourth generation and stringent upper limits on the number of neutrino species. Lower limits on the masses of hypothetical new objects as the supersymmetric particles are also obtained.

Space does not allow to cover the physics of the hadronic jets, that are interpreted as the way in which the constituents appear to the experimenters; we will only quote (Chapter 8) the analogous of the experiment of Geiger and Marsden at these energies and the limits on the diameter of the quark. The limited space does not allow to cover other interesting topics as the discovery of the $B^0 - \bar{B}^0$ oscillations[1].

A new source of antiprotons, ACOL, is now in operation at CERN and will allow an increase in luminosity by an order of magnitude. Both UA1 and UA2 experiments are in the process of being substantially upgraded to provide more stringent tests of the standard model in the coming years. In the same period the Fermilab Tevatron Collider, that started operation $\sqrt{s} = 1.8$ TeV, will be operational. Certainly collider physics will continue to provide existing results in the near

2. THE INTERMEDIATE VECTOR BOSONS. EXPECTATIONS AT THE $\bar{P}P$ COLLIDER

Beta decays of nuclei, originally observed at the end of the last century, are interpreted as beta decays of neutrons or protons bound in the nucleus:

a. $n \rightarrow p + e^- + \bar{\nu}_e$; $p \rightarrow n + e^+ + \nu_e$

We know today that the beta decays of the nucleons are not yet elementary processes but are due to the beta decay of quarks bound in the nucleons:

b. $d \rightarrow u + e^- + \bar{\nu}_e$; $u \rightarrow d + e^+ + \nu_e$

The intermediate vector bosons W^+ and W^- are predicted by the Electroweak theory to be the mediators of these processes. At the lowest order the Feynman graphs are shown in Fig. 1.

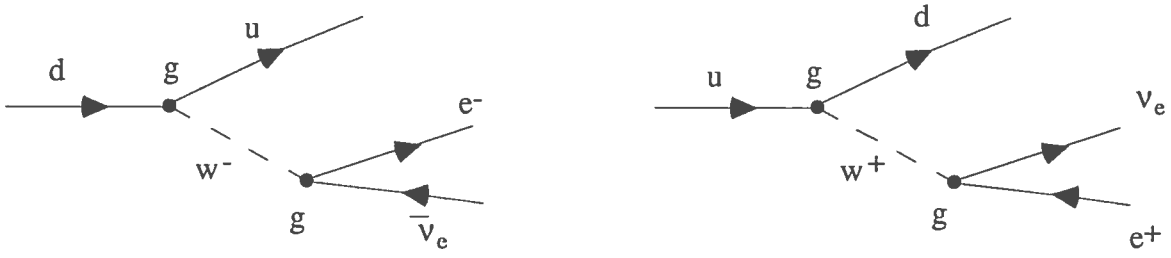

FIGURE 1

In both graphs the quarks in the initial and final states have the same colour. The corresponding matrix element is:

$$M = \left[\frac{g}{\sqrt{2}}\bar{\nu}_e\gamma^\lambda(1-\gamma^5)e\right]\frac{1}{M_W^2 - q^2}\left[\frac{g}{\sqrt{2}}\bar{d}_c\gamma_\lambda(1-\gamma^5)u\right] \qquad (1)$$

where g is the coupling constant, M_W the mass of the W, q^2 the square of the four-momentum transfer and the particle symbols represent the corresponding (relativistic) spinors. Universality of the coupling i.e. the same g in both lepton and quark current terms is obtained, as shown by Cabibbo, introducing substantial mixing amongst the charge -1/3 quarks (d_c is the Cabibbo rotated down quark).

Note that the propagator factor $1/M_W^2 - q^2$ is the probability that a W moves from one vertex to the other of the graphs of Fig. 1. When the energy is very small with respect to the W mass $\left(q^2 << M_W^2\right)$ the W cannot move significant distances and the interaction is effectively in a point. We are in the limit the four-field Fermi point interaction. The propagator is effectively a constant: $1/M_W^2$, and we can identify the Fermi constant G_F:

$$\frac{G_F}{\sqrt{2}} = \frac{g^2}{8M_W} \qquad (2)$$

Note that g has the same order of magnitude as the fine structure constant α (the coupling of the electromagnetic interaction), G_F is much smaller because M_W is large.

We finally remind that the current terms have a V - A structure as is immediately visible in (1). This implies that the W has spin-parity $J^P = 1^-$ and that it couples only with **fermions** (quarks and leptons) with **negative** helicity (spin antiparallel to the velocity) and **antifermions** with **positive** helicity. The test of this important aspect (**parity violation**) of the theory will be described in Sect. 4.4.

W^+ and W^- can be produced from an hadronic initial state by the graphs shown in Fig. 2.

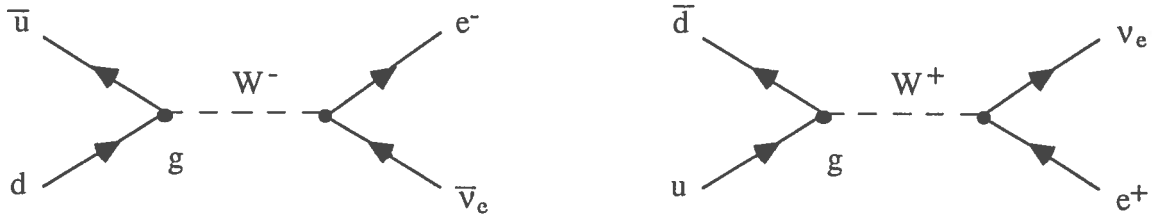

FIGURE 2

Of course different final states as $\nu_\mu\mu$, $\bar{u}d$ etc are possible. Note that also now the quark and the antiquark in the initial state must have the same colour. Due to these graphs the cross sections of the processes:

c. $\bar{u}d \rightarrow e^-\bar{\nu}_e$; $\bar{d}u \rightarrow e^+\nu_e$

have a resonance at $\sqrt{\hat{s}} = M_W$, where $\sqrt{\hat{s}}$ is the energy in the centre of mass of the quark antiquark system.

$$\sigma(\bar{u}d \rightarrow e^-\bar{\nu}_e) \alpha \frac{\Gamma_i \Gamma_f}{\left(\sqrt{\hat{s}} - M_W\right)^2 + \left(\frac{\Gamma}{2}\right)^2} \qquad (3)$$

where Γ is the total width, Γ_i and Γ_f the partial widths in the initial and final states respectively. SU(2) x U(1) gives the following definite predictions:

$$M_W^2 = \frac{A^2}{1-\Delta r} / \operatorname{sen}^2\vartheta_W \quad , \quad A^2 = \frac{\pi\alpha}{\sqrt{2}\,G_F} \qquad (4)$$

From the values of the fine structure constant and of the Fermi constant, known with high accuracy form low energy precision measurements, we obtain[2]:

$$A^2 = (37.2810 \pm 0.0003)^2\ GeV^2 \tag{5}$$

Δr contains the higher order radiative corrections, it is calculated by the Electroweak theory[3]:

$$\Delta r = 0.0711 \pm 0.013 \tag{6}$$

The Weinberg angle is known from low energy measurements, mainly from the ratio of neutral current and charged current neutrino reactions[4]:

$$sen^2\vartheta_W = 0.231 \pm 0.004\ (stat) \pm 0.005\ (syst) \tag{7}$$

With these values the expected value of the mass of the W is:

$M_W = 80.3 \pm 0.9$ GeV

The Electroweak theory gives also a prediction for the total width:

$\Gamma_W \approx 2.6$ GeV

(the precise value depends on the unknown mass of the top quark).

In practice processes c) cannot take place because quarks are not found free in Nature, but only inside the hadrons. We will then consider a high energy proton beam colliding against a high energy antiproton beam. Both beams can be considered in a first approximation as wide band parton $(q, \bar{q}, g)$ beams.

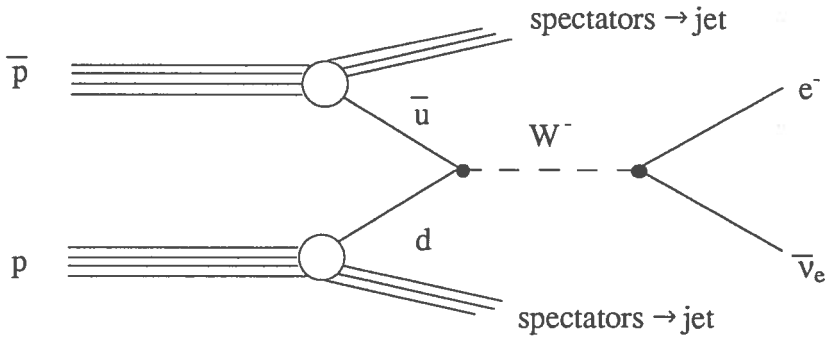

FIGURE 3

In the rare case when an $\bar{u}$ quark of the antiproton closely encounters a d quark of the same colour of the proton, the process depicted in Fig. 3 happens: a W is produced that immediately (after a time $1/\Gamma_W$) decays for example in $e\nu_e$. The process has a sharp resonance at $\sqrt{\hat{s}} = M_W$. In a good approximation we can forget the motion of the quarks transverse to the beam; if x_d is the

fraction of the proton momentum taken by the d quark, and $x_{\bar{u}}$ the fraction of the antiproton momentum taken by the $\bar{u}$ the energy squared in the parton centre of mass is:

$$\hat{s} = x_d \cdot x_{\bar{u}} \cdot s \qquad (8)$$

where s is the energy squared in the $p\bar{p}$ centre of mass.

When an $\bar{u}$ and a d annihilate into a W the proton and antiproton remain in a coloured unstable state; each of them must rearrange its state "hadronizing" and giving origin to a jet of hadrons that move at small angle with original direction: two jets (spectator jets) at low p_T (p_T is the momentum transverse to the beams direction) are observed.

The calculation of the cross section of process d) was done by G. Altarelli at al.[5] with QCD; knowledge of the parton distribution functions in the nucleon (structure functions) is needed. These functions have been measured by deep inelastic lepton scattering at low energies and must be evolved to high energies taking into account QCD scale violations. Fig. 4 shows the relevant quark structure functions. u_v and d_v are the valence quark, s is the "sea" contribution, that contains both quarks and antiquarks. Notice that at the CERN collider energy $\sqrt{s} = 630\ \text{GeV}$, the value of x at resonance is $x = M_W / \sqrt{s} = 0.13$, a value where the valence quark completely dominate.

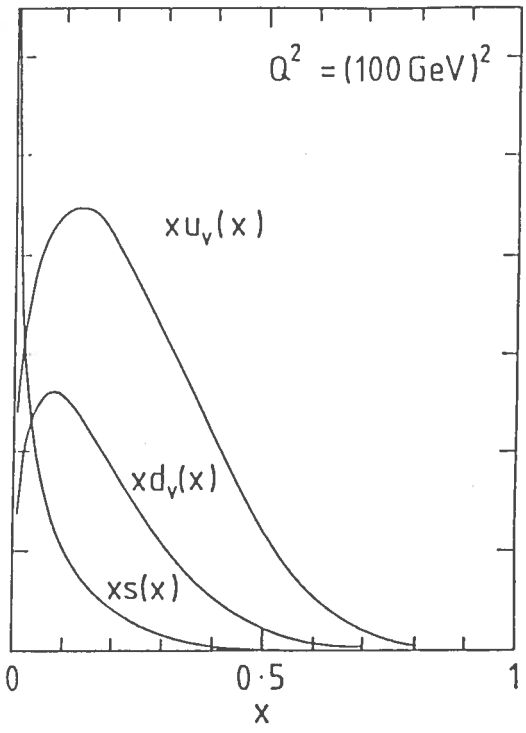

Fig. 4

We are then entitled to think that the interacting quark was in the proton, the interacting antiquark in the antiproton. This is important to be able to observe the asymmetry predicted by V - A (parity

violation).

The expectation for the cross section from QCD calculation at $\sqrt{s}$ = 630 GeV is:

$$\sigma(\bar{p}p \rightarrow W \rightarrow e\nu) = 570^{+\ 180}_{-\ 100}\ pb \qquad (9)$$

a value that is of the order of 10^{-8} of the total cross section.

We turn now to the neutral vector boson, Z^0. It is needed because neutral currents are observed, i.e. processes of the type:

$\nu_\mu N \rightarrow$ hadrons (+no μ)

The relevant Feynman graphs are:

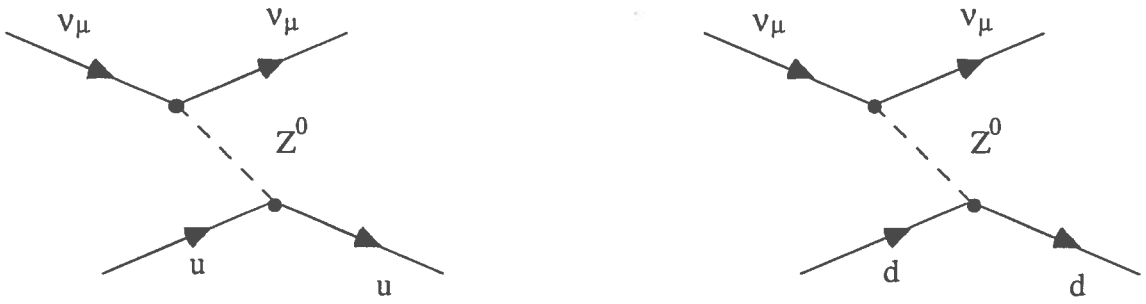

FIGURE 5

and again allow the production of Z^0 in $p\bar{p}$ collisions:

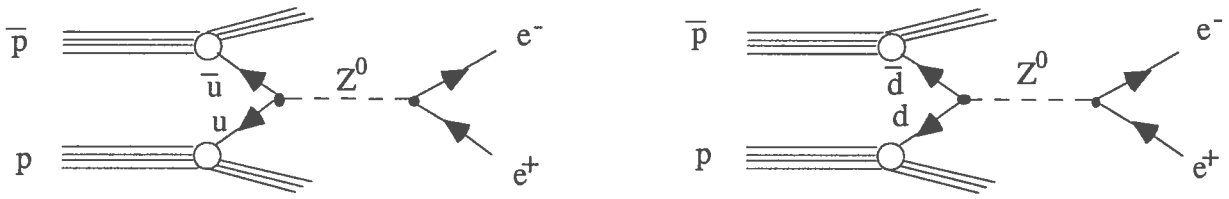

FIGURE 6

Again the quark and antiquark in the initial state must have the same colour and again other final states are possible ($\mu^+\mu^-$, $\tau^+\tau^-$, $u\bar{u}$, $d\bar{d}$, etc). Note that in this case two different processes ($u\bar{u}$ and $d\bar{d}$ annihilation) contribute to the Z^0 production.

SU(2) x U(1) gives clear predictions for the mass

$$M_Z = \frac{M_W}{\cos \vartheta_W} = 91.6 \pm 0.7\ GeV$$

and the total width

$\Gamma_Z \approx 2.6$ GeV

Again the expected value of the cross section is more uncertain (QCD calculation)[5]:

$$\sigma(\bar{p}p \rightarrow Z^0 \rightarrow e^+e^-) = 54^{+17}_{-11}\ \text{pb} \qquad (10)$$

expected at $\sqrt{s} = 630$ GeV, a value an order of magnitude smaller than for $W \rightarrow e\nu$.

In summary the production of the intermediate vector mesons at the $p\bar{p}$ collider is a rare process ($10^{-8} \div 10^{-9}$); their observation requires a rejection power against background at least of 10^{10}. The more frequent final states of the IVB's are $q\bar{q}$ states (about 70%), experimentally observed as two hadronic jets. Unfortunately the background due to gluon-gluon, gluon-quark and quark-antiquark scatterings is very high, two order of magnitude higher than the signal. An accurate measurement of the jet-jet invariant mass should allow to observe resonance peaks at the W and Z^0 masses, but the experimental resolution $\sigma(M_{jj}) \sim 8$ GeV is still too poor to allow a clear identification of the peaks (UA2 has indeed observed a shallow hump in correspondence to the non resolved W and Z masses[6], UA1 is building a "compensated" calorimeter that will largely increase its accuracy in jet energy measurements).

In a much more favorable situation are the leptonic final states. For the W:

$$W \rightarrow \begin{cases} e\nu_e \\ \mu\nu_\mu \\ \tau\nu_\tau \end{cases}$$

where both the charged lepton (e, μ or τ) and the neutrino have a **high p_T** (momentum component perpendicular to the beams) and are **isolated** (meaning that no other energetic particle is produced near to their direction). For the Z:

$$Z \rightarrow \begin{cases} e^+e^- \\ \mu^+\mu^- \\ \tau^+\tau^- \end{cases}$$

the signature being here **two isolated high p_T leptons** of opposite charge.

In both cases the debris of the "spectators" are present in the final state ("underlaying event") but can be easily distinguished because their p_T is much smaller (typically smaller than 1 GeV). Occasionally, as we will see, the initial quark or antiquark can radiate a gluon: a high p_T jet appears in this case in the final state in addition to the two leptons.

The "**isolation**" of a track can be defined quantitatively. The UA1 definition is in the space $(\phi, \eta = -\ln \text{tg}\, \vartheta/2)$ where ϕ is the azimuth around the beam axis and ϑ the angle with the beam; the pseudorapidity variable η is used because the track density in η is much more uniform than in ϑ. A track is defined to be isolated if the energy flux in a cone of given semiaperture

$\Delta R = [\Delta\phi^2 + \Delta\eta^2]^{1/2}$ around the track is less than a given value E_{max}. The specific value of ΔR and E_{max} depend on the particular case considered, as we will see later.

As we will see all the before mentioned final states (with the exception of $Z^0 \rightarrow \tau\tau$) have been clearly observed with a very small background. Let us now consider the measurements of the IVB's masses and the relative accuracy. In the Z^0 case we observe an $e^+ e^-$ pair or a $\mu^+ \mu^-$ pair and measure the energy E_1 and E_2 of the leptons and the angle ϑ between their directions. The invariant mass of the system is:

$$m = \left(4E_1E_2 \operatorname{sen}\frac{\vartheta}{2}\right)^{1/2} \tag{11}$$

and the related resolution:

$$\frac{\sigma_m}{m} = \frac{1}{2}\left[\left(\frac{\sigma_1}{E_1}\right)^2 + \left(\frac{\sigma_2}{E_2}\right)^2 + \left(\frac{\sigma_\vartheta}{\operatorname{tg}\frac{\vartheta}{2}}\right)^2\right]^{1/2}$$

The angle ϑ is generally big and $\operatorname{tg}\frac{\vartheta}{2}$ has value around one; as the directions of the charged tracks are accurately measured, σ_ϑ is of the order of 10^{-2} and the contribution of the angle measurement resolution is negligible. As on the other hand E_1 and E_2 are of the same order:

$$\frac{\sigma_m}{m} = \frac{1}{\sqrt{2}}\frac{\sigma_E}{E}$$

We must at this point distinguish the electron from the muon case. The energy of the electron is measured by the calorimeters with a resolution $\sigma_E / E = 16\% / \sqrt{E}$ (with E in GeV) i.e. $\sigma_E / E = 2\%$ for $m = 90$ GeV ($E = 45$ GeV). In conclusion the resolution of the measurement of the Z mass in the electron channel is $\sigma_m = 1.4$ GeV. The muons, on the other hand, are not observed by the calorimeters, their energy (better their momentum) is measured by a magnetic spectrometer. The resolution is typically $\sigma_p / p = 0.5\% \cdot p$ (with p in GeV) that is 22.5% at 45 GeV (the sagitta of 1 m long track in 0.7 T magnetic field is 6 mm). The corresponding resolution for the Z^0 mass is $\sigma_m = 14$ GeV an order of magnitude worse than the electron channel.

The resolution values quoted above refer to the single measurement and can of course be reduced increasing the statistical sample. The ultimate resolution will be determined by the systematics that will be discussed in Sect. 4.2.

The measurement of the W mass is different because only the charged lepton is directly observed. The charged lepton momentum in the W centre of mass frame is obviously $p_e = M_W/2$. If ϑ^* is the angle between the charged lepton and the beam and we neglect for the moment the transverse motion of the W, the transverse momentum $p_T^e = (M_W/2)\operatorname{sen}\vartheta^*$, is the same in the

W rest frame and in the laboratory frame. From the known decay angular distribution of the W $dn/d\vartheta^*$, one can obtain the p_T^e distribution simply with a coordinate transformation:

$$\frac{dn}{dp_T^e} = \frac{dn}{d\vartheta^*} \cdot \frac{d\vartheta^*}{dp_T^e} = \frac{1}{\left[\left(\frac{M_W}{2}\right)^2 - p_T^{e\,2}\right]^{1/2}} \cdot \frac{dn}{d\vartheta^*} \tag{12}$$

As one can see the "Jacobian" of the transformation has a peak (the "Jacobian peak") at $M_W/2$; the presence of this peak in the data gives direct evidence for the W, its position allows a determination of its mass. The transverse motion of the W smears the peak and can alter its position in a way dependent on dn/dp_T^W. To avoid the consequent model dependence of the evaluation of the mass the momentum of the neutrino should be determined. This can be achieved by measuring the momenta of all the charged and neutral particles produced in the interaction. As the neutrino does not interact with the detector, its momentum can be obtained, applying momentum conservation, from the overall momentum unbalance. The "measurement" of the "missing momentum" is achieved by UA1 with a calorimeter that is hermetic. Unfortunately complete hermeticity cannot be achieved: particles at small angle with the beams escape detection; in practice only the transverse components of the missing momentum $\left(\vec{p}_T^{\,miss}\right)$ are determined. An independent signature of W events is the presence of the Jacobian peak in the p_T^{miss} distribution.

We can now define the "transverse invariant mass":

$$m_T^{ev} = \left[2p_T^e p_T^{miss}(1 - \cos\phi)\right]^{1/2} \tag{13}$$

where ϕ is the angle between the two leptons in the transverse plane. The distribution of m_T^{ev} has a peak only a few GeV lower than M_W. It is only in these few GeV that the model dependence of dn/dp_T^W enters.

3. THE DETECTOR

The discussion of the previous chapter allows us to lay down the main characteristics to demand to the detector. It must be able to identify the elementary objects produced by the collision and to measure their energy, momentum and charge. The elementary objects are: a) the charged leptons, the **electron** (identified by its characteristic shower in a heavy material), the **muon** (identified by its ability to penetrate deeply into matter) and the **tau** (identified by the shape of the jet produced by its fast (lifetime = 0.33 ps) decays into hadrons; b) the **neutrinos** (identified by an overall momentum unbalance); c) **quarks** and **gluons** experimentally measured as hadronic **jets** (identified by the tracking chambers and by the calorimeters).

The UA1 apparatus consists of different layers of different detectors (Fig. 7). The innermost is a cylindrical drift chamber around the beam pipe 5.8 m long, 2.3 m in diameter; it is called the

Central Detector[7] (C.D.) and provides a three-dimensional picture of the charged tracks, down to 0.2° with respect to the beams. It is immersed in a uniform dipole magnetic field horizontal and perpendicular to the beams (B = 0.7 T); it provides the momentum measurement with a typical resolution $\Delta p/p = 0.005\ p$ (p in GeV).

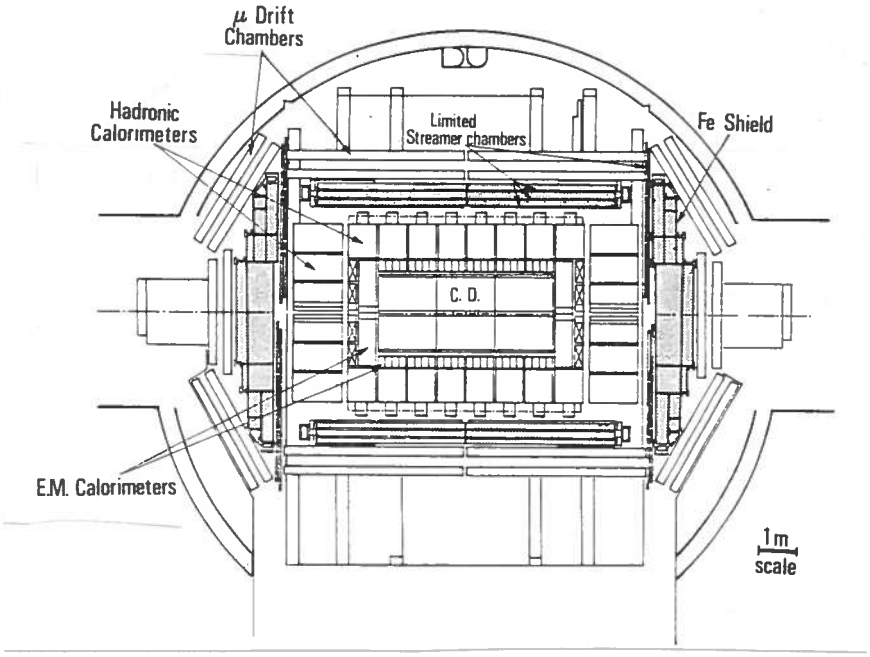

FIGURE 7
The UA1 detector

Outside the lateral surface of the Central Detector one finds the central electromagnetic[8] calorimeter, which covers the polar angle interval between 25° and 155° and 2π in azimuth. It consists of two half cylinders on the two sides, each composed of 24 elements, the "gondolas". A gondola is a lead-scintillator sandwich of 26.6 radiation lengths with independent read-out of four longitudinal samplings of 3.3, 6.6, 10.1 and 6.6 r.l. respectively. The energy deposited in the gondola is measured with an accuracy $\Delta E / E = 16\% / \sqrt{E}$ (E in GeV). Each gondola covers the angle interval $\Delta\vartheta = 5°$, $\Delta\phi = 180°$.

The two end-cap calorimeters, the "bouchons" consist of 32 "petals" of lead-scintillator sandwich. They are 27 r.l. thick, segmented four times in depth. The energy resolution is the same as that of the gondolas. With the gondolas they provide coverage down to 5° to the beams, additional forward located calorimeters provide coverage down to 0.2°[8].

The electromagnetic calorimeters are located inside the magnetic field. The yoke of the dipole magnet is outside the gondolas and is made of iron plates separated by plastic scintillator plates to form the central hadronic calorimeter[9]. Similar structures outside the bouchons from the forward hadronic calorimeters. The calorimeters are read-out in two separated longitudinal samples. The central one is 5 absorption lengths thick, the forward ones 7 absorption lengths. Their granularities are $\Delta\vartheta \times \Delta\phi = 15° \times 18°$ and $5° \times 10°$ respectively. Their energy resolution is $\Delta E / E = 0.8 / \sqrt{E}$ (E in GeV). Electron and photon showers in the electromagnetic calorimeters are completely absorbed, hadrons penetrating in the heavy material of the calorimeters interact giving origin to a

hadronic shower; a good fraction of their energy is deposited in the electromagnetic calorimeter, the rest in the hadronic one. Rarely tails of the hadronic shower emerge from the back of the calorimeters. Iron shields 60 cm thick on the sides, more than 1 m thick in the forward direction completely absorb these tails. Limited streamer tubes detectors[10] layers instrument the shields allowing the tracking of penetrating charged particles, the muons. On the sides the iron is magnetized. Outsides the iron shielding two planes of drift chambers[11], separated by a 60 cm distance, give accurate measurements of the muon track coordinates. Each plane measures twice each of two orthogonal coordinates. The muon detection system covers the full interval in azimuth and between 5° and 175° in polar angle, it allows also to determine the deflection of the track in the magnetic field in the yoke and in the lateral walls thus providing and independent measurement of the muon momentum.

Electrons are identified by the characteristic longitudinal development of the shower and by the presence of an associated charged track. The principal background is due to one (or more) π° near to a medium energy $\pi^\pm$; the electromagnetic shower of the photons from the π° overlapped to the hadronic shower of the charged π can mimic a truly electromagnetic shower. A comparison of the total energy of the shower with the momentum of the charged track as measured in the C.D. eliminates part of this background. This background is of course normally near or into the hadronic jets. In conclusion high p_T, isolated electrons are easy to identify (discriminating power against jets ~40.000), much more difficult at lower p_T or near to the jets, impossible inside jets.

Muons are identified by the presence of a charged track in the muon chambers associated with a charged track in C.D. The principal background is due to K or π decays into a muon in C.D., when the kink of the track is not observed. In these cases the track momentum is overevaluated and an oppositely directed "missing momentum", interpreted as a neutrino, is generated. The background is controlled by an accurate study of the track quality in the C.D. and comparing the two measurements of its momentum. The event sample containing one muon is 80% pure at p_T = 20 GeV, 25% pure at p_T = 6 GeV. In conclusion isolated high p_T muon can be easily separated from background but this becomes increasingly difficult as p_T decreases. On the other hand it is possible to identify muons even inside jets, opening the route to heavy flavour (bottom and top) physics.

A **jet** appears clearly as a localized energy deposit in the calorimeters; all the hadronic events with total transverse energy E_T bigger than 20-30 GeV consist on two or more jets, as the example shown in Fig. 8. This observation leads immediately to interpret jets as manifestations of the quarks and of the gluons. On the other hand the identification of the energy and direction of the jets with those of the parton is subject to uncertainties both experimental and theoretical; the most important are the non linear response of the calorimeter at low energies, the different response to a π° (electromagnetic) and to a $\pi^\pm$ (hadronic) of the same energy, the uncertainties on the soft tails of the fragmentation, the subtraction of the contribution of the underlaying event.

Tau leptons are identified[12], in their hadronic decays, by the narrow, low multiplicity shape of the jet.

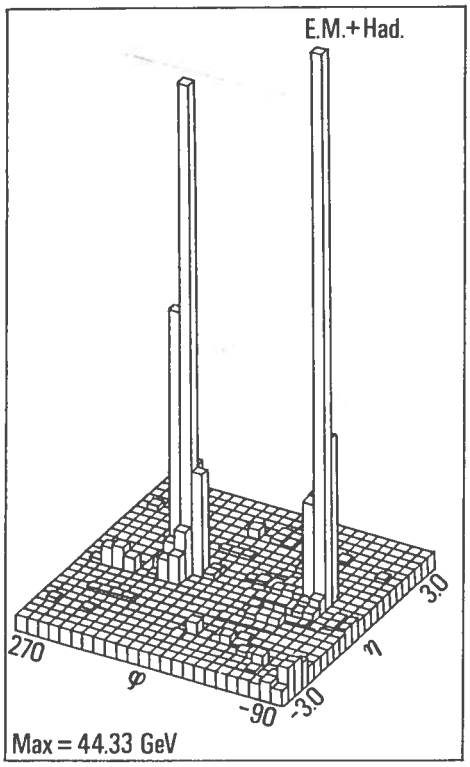

FIGURE 8
"Lego plot" of a two jet event. Energy deposit in the calorimeter cells in the φ, η space.

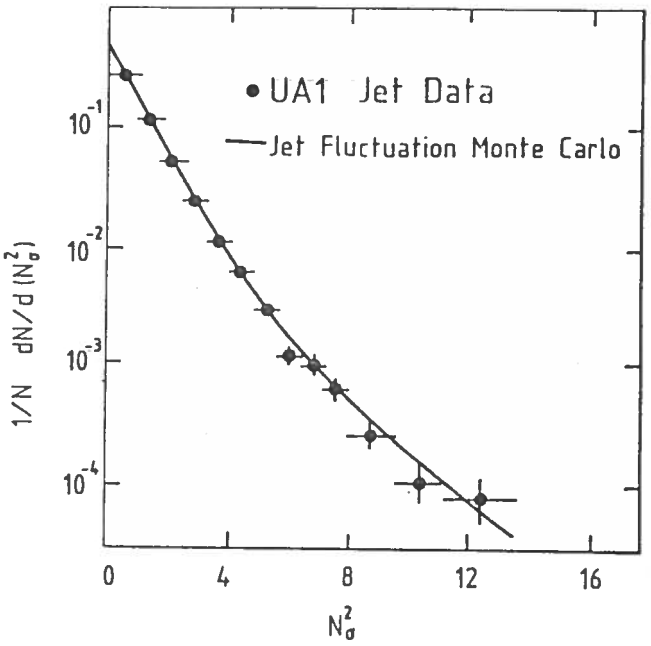

FIGURE 9

The presence of **one or more neutrinos** (or other unknown non interacting particles) can be inferred by measuring the total momentum vector of the interacting particles and obtaining values different from zero (outside the errors). In practice even providing a coverage down to a fraction of a degree, it is impossible to measure the energy of the secondaries at small angle with the beams; the longitudinal component of the total momentum can not be measured. On the other hand undetected particles give a negligible contribution to the transverse momentum allowing its determination with good accuracy. If E_i is the energy deposited in the i cell of the calorimeter and $\vec{u}_i$ the versor of the cell from the interaction point we can define the energy (momentum) vector in the cell: $\vec{E}_i = E_i \vec{u}_i$ and its component in the transverse plane $\vec{E}_{iT}$; the missing transverse momentum is then:

$$\vec{p}_T^{\,miss} = -\sum_i \vec{E}_{iT} - \vec{p}_T^{\,\mu}$$

where $\vec{p}_T^{\,\mu}$ is the transverse momentum of the muons (that deposit very small energy in the calorimeters).

Events with high $\vec{p}_T^{\,miss}$ are the of outstanding importance, as they can signal the presence of new physics; the knowledge of the resolution function in the $\vec{p}_T^{\,miss}$ measurement is as a

consequence extremely relevant. The study of a sample of events where neutrinos are not expected allowed UA1 to determine this function that is a gaussian with:

$$\sigma\left(p_T^{miss}\right) = 0.7\sqrt{|E_T|} \tag{14}$$

where $|E_T|$ is the scalar sum of the transverse energies. It is shown, as a function of $N_\sigma\left(p_T^{miss}\right) = 0.7\sqrt{|E_T|}$ i.e. the number of standard deviations, in Fig. 9 where the data are compared with the expectations due to the fluctuations in the measurement of the energy of the jets. As it can be seen by the agreement, the resolution function is completely under control.

4. THE INTERMEDIATE VECTOR BOSONS

4.1 THE DATA SAMPLE

In a series of data taking periods between 1982 and 1985 UA1 collected data at $\sqrt{s} = 546$ GeV for an integrated luminosity of 118 nb^{-1} and at $\sqrt{s} = 630$ GeV for 568 nb^{-1}. The total of 686 nb^{-1} corresponds to about 50 x 10^9 $\bar{p}p$ collisions.

The main triggers, simultaneously operating, have been the following:

1. One ore more electromagnetic clusters with E_T bigger than a given threshold (depending on running conditions, typically 10 GeV);
2. One or more hadronic jets with E_T bigger than a given threshold (typically 25 GeV);
3. Left-right E_T unbalance and at least one jet with $E_T > 25$ GeV;
4. One or more muons;
5. Total E_T bigger than a given threshold;
6. Other physics triggers.

4.2 $W \rightarrow e\nu$ AND $Z^0 \rightarrow e^+ e^-$

In both cases an isolated high p_T electron is searched for. The selection criteria[13] are tuned to obtain a high rejection against jets (π^0 $\pi^\pm$ overlap) and a reasonable high efficiency for electrons. The main cuts are the following:

1) One electromagnetic cluster with calibrated $E_T > 15$ GeV;

2) A charged track in the C.D. associated in position and angle with the electromagnetic cluster with momentum consistent with $p_T > 15$ GeV;

3) Longitudinal development of the shower, as measured in the 4 samplings, compatible with electromagnetic nature;

4) Small (< 0.6 GeV) energy deposit in the first hadronic compartment;

5) Isolation, requiring both p_T (C.D. measurement) and E_T (calorimeter measurement) in $\Delta R < 0.7$ to be smaller than 3 GeV.

The efficiency of all these cuts is around 70% for electrons from IVD's decay. Having selected one electron we now look for missing p_T to select W's, for a second electron to select Z^0's.

In the W selection $p_T^{miss} > 15$ GeV is requested, giving the final sample of 299 events (the overall selection efficiency is around 60%). The Z^0 sample is obtained requiring a second electromagnetic cluster with less tight selection criteria (isolation with higher threshold and transverse energy of the electron > 8 GeV); it consists of 33 events (selection efficiency ~70%).

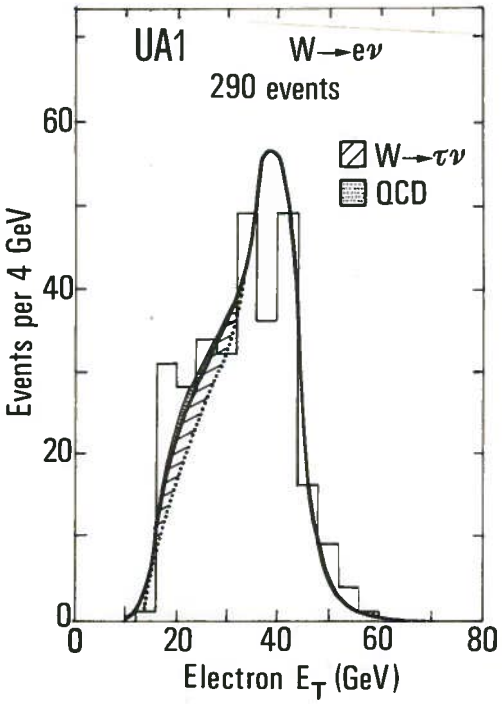

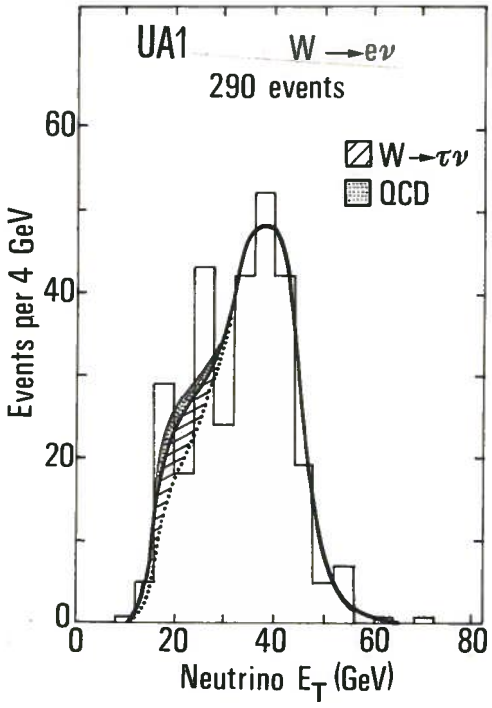

FIGURE 10 **FIGURE 11**

Shaded parts show expected background contributions from jet fluctuations and from $W \to \tau\nu$. Curves are predictions for $M_W = 82.7$ GeV.

Fig. 10 and 11 show the distributions of p_T^e and p_T^ν respectively. The Jacobian peaks are clearly seen out of the background dominant at low values. The background in the W sample due to jets misidentification is evaluated extrapolating the background dominated low p_T distribution into the sample region. It amounts to 3% of the sample. A second background source comes from the W itself through the decay $W \to \tau\nu$, when the τ decays into one electron or misidentified hadrons. Knowing the decay properties of the W it can be reliably calculated and it amounts to 6% of the data. In conclusion the sample of 299 W candidates contains 26.1 ± 2.6 background events. These events are all at low values of p_T^e and p_T^ν. For the determination of M_W a further cut: $p_T^e > 30$ GeV, $p_T^\nu > 30$ GeV is applied to obtain a background free sample of 149 events.

The transverse mass (M_T) distribution is shown in Fig. 12. To extract M_W from the data[14], Monte Carlo calculations are done with different values of M_W and fixed value of Γ_W near to expected one. The simulation takes into account the expected transverse and longitudinal motions of the W (and associated QCD uncertainties). The best fit is shown in Fig. 12. The same calculation is used to evaluate systematic errors, obtaining[14]:

UA1 $M_W = 82.7 \pm 1.0$ (stat) $\pm$ 2.7 (syst) GeV (15)

For comparison UA2 finds (with similar statistics)[15]

UA2 $M_W = 80.2 \pm 0.8$ (stat) $\pm$ 1.3 (syst) GeV (15)

Both values agree perfectly with the expectations (see Chapter 2). Note that the error is dominated by the systematics due to uncertainty on the absolute energy scale.

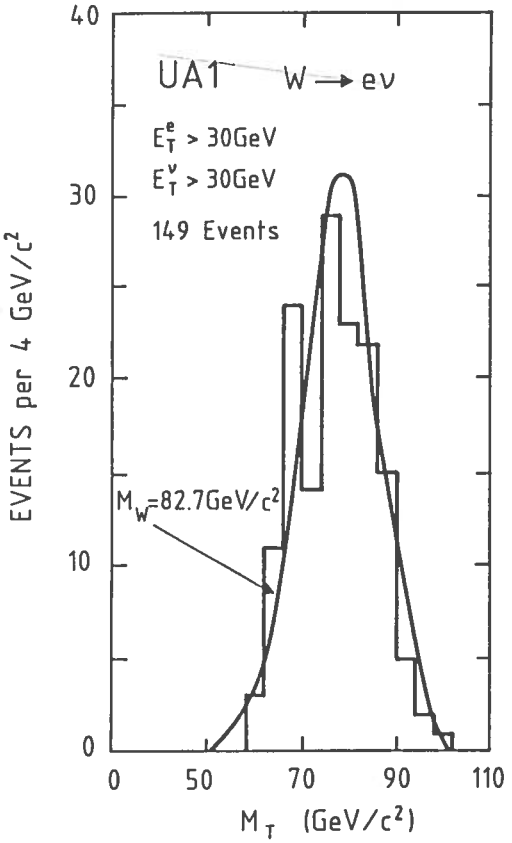

FIGURE 12
Transverse mass distribution for W candidate events with well measured electron and leptons transverse momenta bigger that 30 GeV.

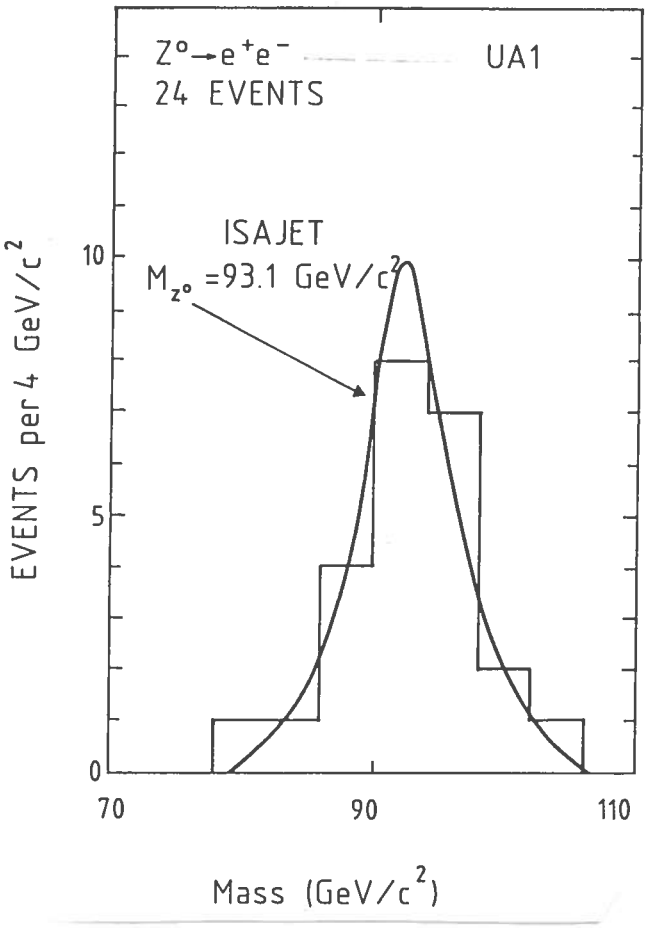

FIGURE 13
e^+ e^- invariant mass distribution for Z^0 candidates with well measured electrons.

Turning now to the width, we note that for both experiments the width of the resolution function is comparable with the expected natural one Γ_W. The uncertainties on the resolution function in these conditions allow only to put upper limits on Γ_W[14,15]:

UA1 $\Gamma_W < 5.4$ GeV (16)

UA2 $\Gamma_W < 7.0$ GeV (16)

at 90% c.l.

Let us now consider the 33 events Z^0 sample that is practically free from background (evaluated number of background events is 0.2 ± 0.02). To determine M_Z a subsample of 24 events with both electrons accurately measured is selected. The two-electron invariant mass distribution is shown in Fig. 13. From the fit we obtain[14]:

UA1 $\quad M_Z = 93.1 \pm 1.0 \pm 3.1$ GeV (17)

For comparison[15]:

UA2 $\quad M_Z = 91.5 \pm 1.2 \pm 1.7$ GeV (17)

Both are in perfect agreement with expectations.

Again the dominant error is that on the energy scale, again both experiments give only upper limits for the width; at 90% c.l.[14,15]:

UA1 $\quad \Gamma_Z < 5.2$ GeV (18)

UA2 $\quad \Gamma_Z < 5.6$ GeV (18)

The uncertainties on the energy scale is evaluated to be ±3% for UA1 and ±1.6% for UA2. Both experiments measure the energy deposited by the particles in sampling calorimeters that are sandwiches of active material (scintillator) and passive material (lead or iron). The quantity measured is the total charge collected at the anodes of a number of photomultipliers. This charge results as the final product of a long series of processes: energy loss in scintillator, light emission from the modules of the scintillator; partial collection of the light by the light guides, photoelectric effect at the photocathodes, amplification of the electrons in the P.M. Of course the conversion factor from collected charge to energy lost by the particle must be obtained calibrating the calorimeter cells on an electron and pion beam at different energies. Unfortunately the "calibration constants" are subjected to vary with time due for example to ageing and radiation damage; it is then necessary to monitor continuously their values with light sources and radiative sources. At the hadron colliders a direct, in situ, calibration tool, as that given by $e^+ e^-$ elastic scattering at the $e^+ e^-$ machines, is not in fact available. The complex procedure outlined leads to the residual uncertainty quoted above. The UA2 experiment, having smaller calorimeter cells, was able to recalibrate part of them periodically in a test beam; on the contrary UA1 could not move its large calorimeter cells to a test-beam area.

One of the main target of the upgrade program of both experiments is to obtain a much better control of the systematic. In particular UA1 has developed a new technique, where the ionization charge is directly collected without amplification to this aim.

4.3 COMPARISON WITH THE STANDARD MODEL

Three independent definitions of the Weinberg parameter $\text{sen}^2\vartheta_W$ can be given. The first:

$$\text{sen}^2\vartheta_W = 1 - (M_W/M_Z)^2 \tag{19}$$

is free from radiative corrections and, from the experimental point of view, insensitive to the energy scale error.

The second definition (from (5)):

$$\text{sen}^2\hat{\vartheta}_W = (1 - \Delta r) / A \cdot M_W^2 = (38.65 / M_W)^2 \tag{20}$$

contains the radiative correction term Δr, that is, as we will see, in particular sensitive to the top mass M_t.

The third value is obtained from the ratio of neutral and charged current neutrino interactions. The weighted average of the two must precise experiments[14] is:

$$\text{sen}^2\vartheta^{\nu}_W = 0.232 \pm 0.004 \text{ (stat)} \pm 0.003 \text{ (theor)} \tag{21}$$

The three quantities could be a priory different. Their equality is a definite prediction of the Electroweak theory. Experimentally from (19) we have:

UA1 $\quad \text{sen}^2\vartheta_W = 0.211 \pm 0.025$ (22)

UA2 $\quad \text{sen}^2\vartheta_W = 0.232 \pm 0.027$ (22)

and from (20)[14]:

UA1 $\quad \text{sen}^2\hat{\vartheta}_W = 0.218 \pm 0.005 \pm 0.014$ (23)

UA2 $\quad \text{sen}^2\hat{\vartheta}_W = 0.232 \pm 0.003 \pm 0.008$ (23)

The equality of all the values constitutes a stringent test of the standard model. The agreement is shown in graphical form in the ($M_Z - M_W$, M_Z) plane in Fig. 14. A global fit to the neutrino data and to the W and Z masses gives for the radiative correction term[16]:

$$\Delta r = 0.077 \pm 0.037 \tag{24}$$

This value is consistent with the theoretical one (6); this last value could be different for two main reasons: 1) for high value of the top mass ($M_t > 80$ GeV), Δr decreases becoming negative for $M_t \sim 250$ GeV; this is due to the fact that the graph shown in Fig. 15 gives negative contribution to the W mass proportional to $M_t^2 - M_b^2 \cong M_t^2$ and there is no similar contribution to the Z^0 mass. The result is[3]:

$$\Delta r = 0.0711 - \frac{3\alpha}{16\pi}\left(\cos^2\vartheta_W / \mathrm{sen}^4\vartheta_W\right)\cdot\frac{M_t^2}{M_W^2} \qquad (25)$$

2) new fermion doublets with large mass splitting give similar contribution, decreasing Δr.

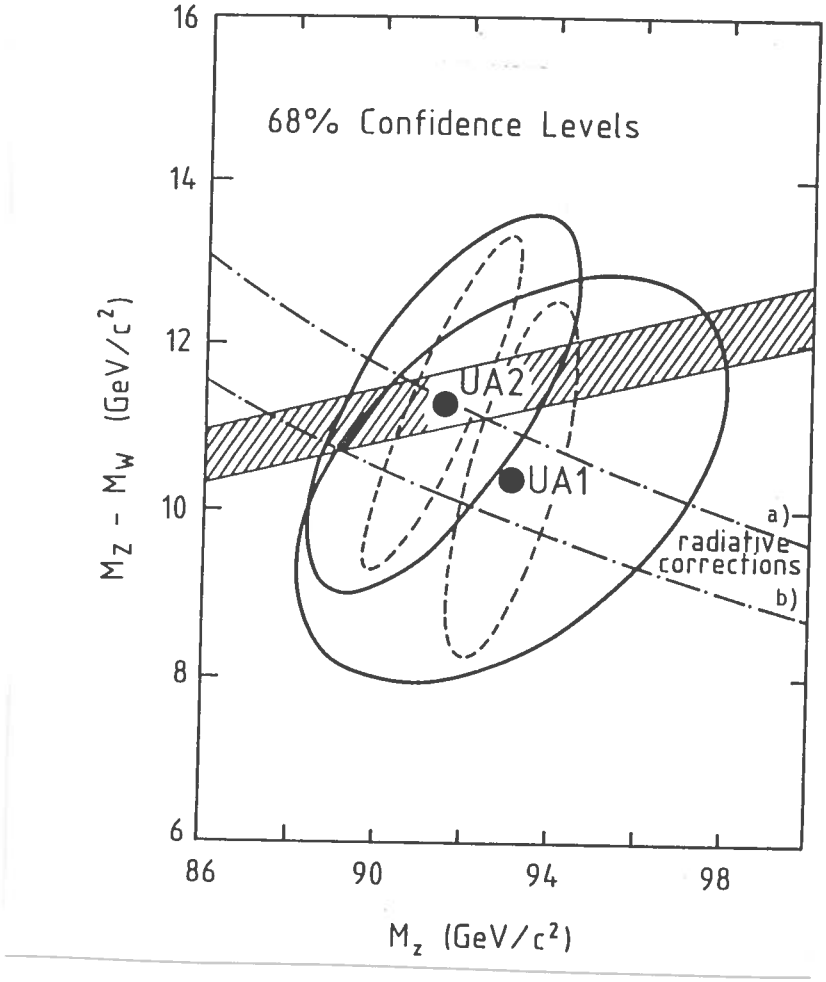

FIGURE 14

Dotted ellipses are 68% c.l. confidence contours taking account only statistical uncertainties, solid ellipses are the same including systematics. Dashed band is the prediction from low energy data. Curve a) S.M. prediction with $\rho = 1$ with radiative corrections, curve b) the same without radiative corrections.

The value (24) with expression (25) allows us to put an upper limit on the mass of the top: $M_t < 180$ GeV (in the hypothesis of the three families).

One of the most important targets of the improved UA1 and UA2 experiments is the precise measurement of Δr. This will allow to limit the mass of the top, if not yet found, or test the number of families, if M_t will be known.

In the minimal Standard Model, considered so far, an isospin doublet of Higgs fields is assumed. This implies equality of the coupling strength of neutral and charged currents. Their ratio:

$$\rho = M_W^2 / \left(M_Z^2 \cos^2 \vartheta_W \right) \tag{26}$$

may be different from 1 for more complicated isospin structures of the Higgs fields. Using (20) to evaluate $\text{sen}^2\vartheta_W$ we have:

UA1[14] $\rho = 1.009 \pm 0.028 \pm 0.020$ (27)

UA2[15] $\rho = 1.001 \pm 0.028 \pm 0.006$ (27)

both perfectly compatible with 1.

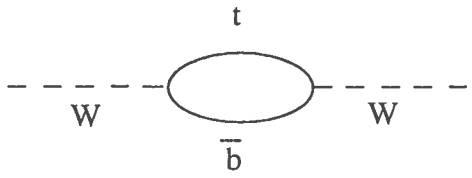

FIGURE 15

4.4 THE PARITY VIOLATION

The V-A coupling of the W implies parity violation of the weak interactions. As a consequence a charge asymmetry will be observed; as we will now see electrons will tend to be emitted forward with respect to incident protons, positrons backward. The charge asymmetry is apparent at CERN collider energies because, as we mentioned in Chapter 1, W production is mainly due to the valence quarks and antiquarks and we may identify the direction of the initial quark with that of the proton beam, the direction of the antiquark with the $\bar{p}$ beam.

V-A coupling fixes the helicity states of the leptons that couples to the W. With reference to Fig. 16

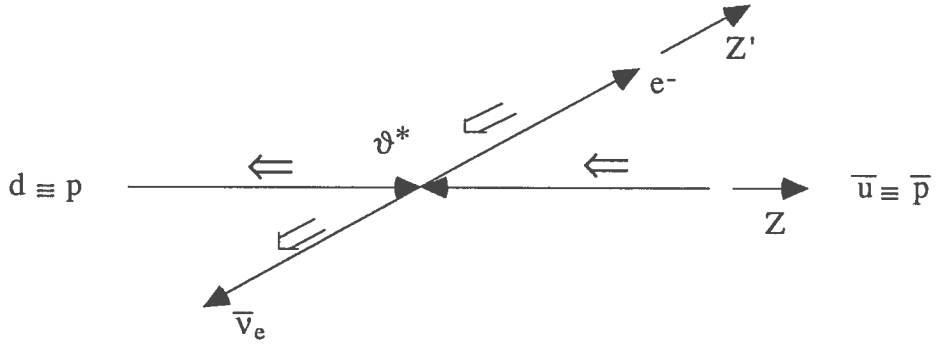

FIGURE 16

we see that the initial state has $J = 1$, $J_z = -1$, i.e. the W is fully polarized with respect to the beam direction. The final state is, on the other hand, $J = 1$, $J_{z'} = -1$. The transition element must then be proportional to the rotation matrix element $d^1_{-1,-1}$, i.e.:

$$\frac{d\sigma}{d\Omega} \alpha \left[d^1_{-1,-1} \right]^2 = \left[\frac{1}{2} (1 + \cos \vartheta^*) \right]^2 \tag{28}$$

where ϑ^* is the angle between e^- and p in the W^- centre of mass, or between e^+ and $\bar{p}$ in the W^+ centre of mass.

Experimentally p_L^ν is not measured, so the transformation to the W centre of mass is not trivial. The problem is solved imposing to the $e\nu$ invariant mass to be equal to M_W. The problem has two solutions for p_L^W but in the great majority of the events only one is physical. Keeping these events and further requiring that the electron charge is well measured we are left with 149 events. The (corrected) angular distribution for this sample is shown in Fig. 17 compared with the prediction of the V-A structure. Notice that non conservation of parity is observed, but V-A is not proven. In fact V+A would give exactly the same prediction.

More generally assuming an arbitrary spin J for the W it can be shown[17] that the following predictions hold:

$$\begin{array}{lll} J = 1 \text{ and } V \pm A & : & \langle \cos\vartheta^* \rangle = \frac{1}{2} \\ J = 0 & : & \langle \cos\vartheta^* \rangle = 0 \\ J > 1 & : & \langle \cos\vartheta^* \rangle \leq \frac{1}{6} \end{array} \qquad (29)$$

From the data in Fig. 17 we can calculate:

$$\langle \cos\vartheta^* \rangle = 0.43 \pm 0.07$$

proving both J = 1 and V ± A coupling (maximum helicity).

The situation is different for the Z^0, that couples to fermions, f, of both helicities. The Z^0 $f\bar{f}$ vertex is in fact proportional to:

$$\frac{g}{\cos\vartheta_W} \gamma_\mu \frac{1}{2} \left(C_V^f - C_A^f \gamma_5 \right)$$

where C_V^f and C_A^f are the vector and axial couplings of fermion f respectively. For the final state $e^+ e^-$, $C_A^e = -1/2$, $C_V^e = -1/2 + 2\,\mathrm{sen}^2\vartheta_W = -0.03$. Should $\mathrm{sen}^2\vartheta_W$ be equal to 1/4, $C_V^e = 0$ and the coupling would have been purely axial, the angular distribution symmetric. The smallness of C_V^e produces a slightly asymmetric angular distribution. To calculate $d\sigma/d\cos\vartheta^*$ we must remind that two processes contribute:

$$u\bar{u} \rightarrow Z^0 \rightarrow e^+e^- \qquad ; \qquad d\bar{d} \rightarrow Z^0 \rightarrow e^+e^-$$

For each of them:

$$\frac{d\sigma}{d\cos\vartheta^*} = \left(C_V^{i\,2} + C_A^{i\,2} \right)\left(C_V^{e\,2} + C_A^{e\,2} \right)(1 + \cos^2\vartheta^*) + 8\, C_V^i C_A^i C_V^e C_A^e \cos\vartheta^* \qquad (30)$$

where i, meaning initial state, can be u or d. The last term gives the asymmetry, depending on C_V^i, C_A^i that are known functions of the Weinberg angle. Fig.18 shows the experimental distribution, where a small asymmetry is observed. If $N^+(N^-)$ is the number of events with $\cos\vartheta^* > 0$ (<0) we have:

$$A = \frac{N_+ - N_-}{N_+ + N_-} = 0.30 \pm 0.15 \qquad (31)$$

This value can be compared with the prediction based in the weighted average of the contribution of the two processes (30) obtaining a measurement of the Weinberg angle.

$$\text{sen}^2\vartheta_W = 0.18 \pm 0.04 \qquad (32)$$

We have still another independent way to measure this important quantity, that will give another check when statistics will be more adequate.

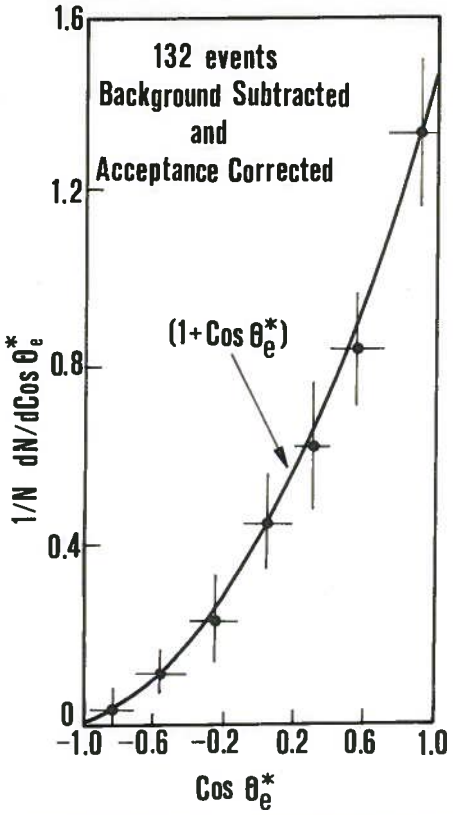

FIGURE 17

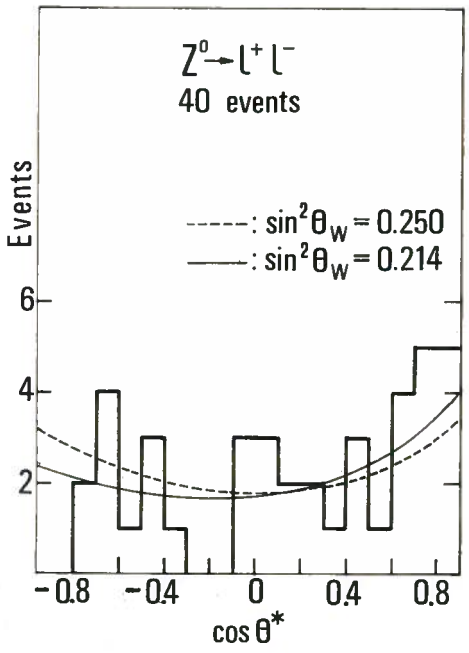

FIGURE 18

4.5 $W \to \mu\nu$ AND $Z^0 \to \mu^+ \mu^-$

Universality requires that equal rates of the IVB's are observed in the electron and muon channels. Experimentally, as discussed above, electron and muons are detected in completely different ways with different backgrounds. This allows a powerful check of the results.

To select the $W \rightarrow \mu\nu$ sample[18,14] an isolated track is required in the external drift chambers matching a high momentum track in the C.D. with $p_T^{\mu} > 15$ GeV and a missing momentum $p_T^{miss} > 15$ GeV. The resulting sample consists on 57 events with negligible background. The reduced events number with respect to the electron channel is due to the limited solid angle covered by the muon trigger. As described in Chapter 3 the momentum of the muon is measured with a sizeable error, about 25% at p = 50 GeV. More precisely the measured, gaussian, quantity is 1/p, hence we consider the inverse transverse mass $1/M_T$. Its distribution is shown in Fig. 19. Fitting the expected shape of the distribution we obtain[14]:

$$M_W = 81.8^{+6.0}_{-5.3}(\text{stat}) \pm 2.6(\text{syst})\ \text{GeV} \tag{33}$$

where the systematic error is due to the uncertainties in the correction of the Central Detector distortions.

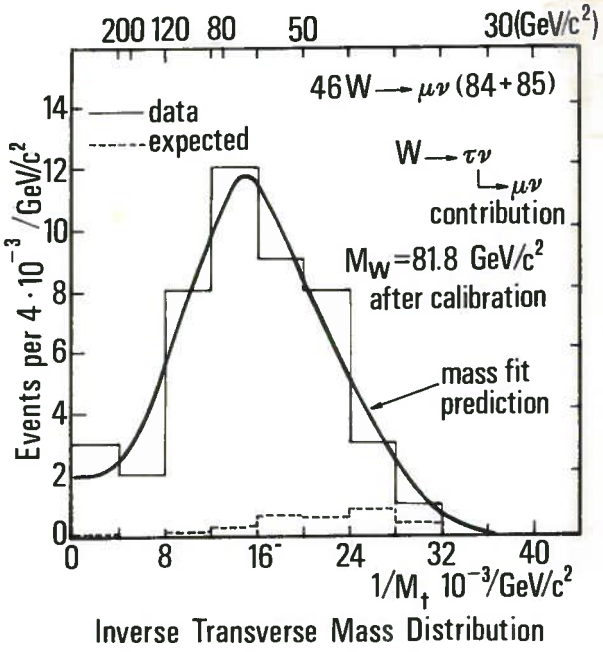

FIGURE 19
Inverse transverse mass distribution for $W \rightarrow \mu\nu$ candidates. Solid curve is the mass fit prediction with $M_W = 81.8$ GeV.

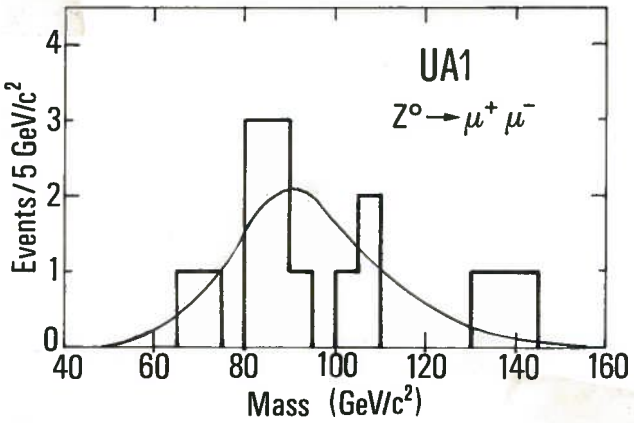

FIGURE 20
The dimuon invariant mass distribution, before the use of momentum balance, for the 18 events for which both μ tracks are well measured. Three events are in over flow. Curve is the fit with M_Z = 94.1 GeV.

Requiring the presence of a second muon with $p_T^{u} > 15$ GeV and such that the dimuon invariant mass $M_{\mu\mu} > 40$ GeV UA1 gets[14] a sample of 18 background free Z^0 events. The $M_{\mu\mu}$ distribution is shown in Fig. 20. Note the asymmetry due to the fact that the resolution is Gaussian in 1/p. The fit gives:

$$M_Z = 94.1^{+8.4}_{-6.6}(\text{stat}) \pm 2.8\,(\text{syst})\,\text{GeV} \tag{34a}$$

By imposing energy-momentum conservation to the whole event a more precise value is obtained:

$$M_Z = 90.7^{+5.2}_{-4.8} \pm 3.2\ \text{GeV} \tag{34b}$$

The muon channel allows independent measurements of the W and Z masses. They are in complete agreement with the (more precise) values obtained in the electron channel.

4.6 $W \to \tau\nu$, THE MISSING ENERGY ROUTE

The hermeticity of the UA1 detector allows a reliable determination of the transverse components of the missing momentum vector $\vec{p}_T^{\,mis}$. As we have seen in Chapter 3 the resolution function on p_T^{mis} is gaussian with $\sigma = 0.7\sqrt{|E_T|}$. Events with high p_T^{mis} are extremely interesting because they contain high p_T neutrinos or, possibly, other non-interacting particles (like photinos, $\tilde{\gamma}$) that should be evidence for new physics. Fig. 21 summarizes the expectations.

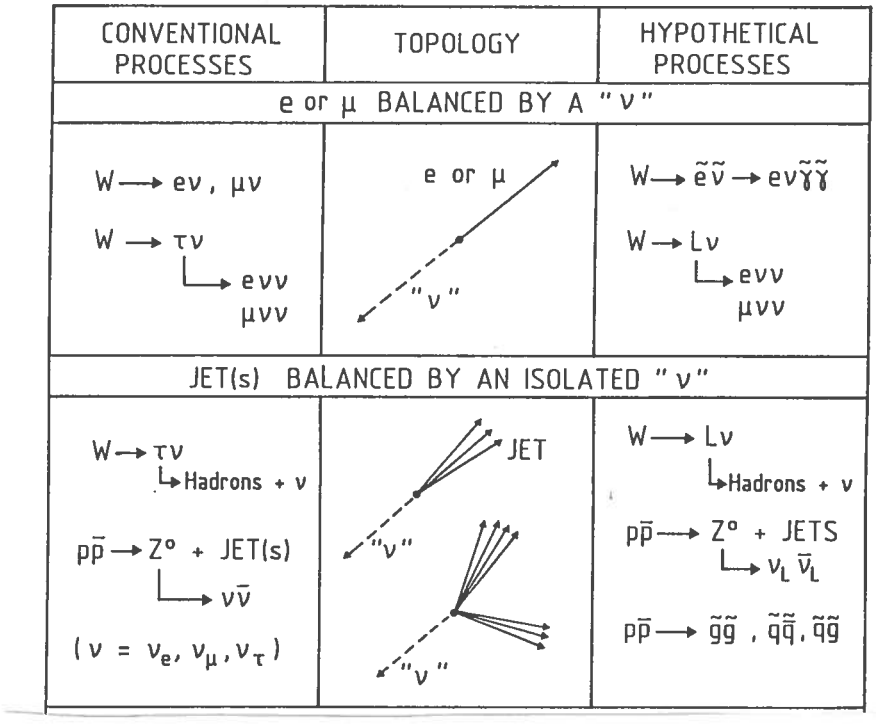

FIGURE 21

The first two topologies, high p_T electron or muon and high p_T^{mis} at large angle, are those previously considered for $W \to e\nu$ and $\mu\nu$. Unknown processes as W decays in scalar electron or muon (predicted by supersymmetry) could contribute (see Sect. 7.2). In the next row "monojet" events are considered: they contain high p_T hadronic jets opposed to p_T^{mis}. We expect contributions from $W \to \tau\nu$ with hadronic decay of the τ; to monojets and multijets we expect also

contributions of Z^0 + jet(s) events, followed by $Z^0 \rightarrow \nu\bar{\nu}$ decay that leads to p_T^{mis}; this is a way to count neutrino species; if more than three generations exist and if neutrino have mass $M_\nu << M_Z/2$ more $Z^0 \rightarrow \nu\bar{\nu}$ channels are open and more missing energy events are expected. If a fourth generation exists and if the decay channel $W^0 \rightarrow L\nu_L$ (where L is the fourth generation charged lepton) is open $(M_L < M_W - M_{\nu_L})$ again additional contributions are expected. Finally the existence of supersymmetric partners of quarks and gluons, the squarks $(\tilde{q})$ and gluinos $(\tilde{g})$ are expected to decay finally into photinos $(\tilde{\gamma})$ massless neutrino-like non-interacting objects.

The main selection criteria for the large missing energy sample are[12]:

1. $p_T^{mis} > 15$ GeV;
2. $p_T^{mis}/\sigma > 4$, i.e. p_T^{mis} at least four standard deviations away from zero. This criterium gives very strong reduction of the background due to the jet energy measurement fluctuations;
3. one or more jets with $E_T > 12$ GeV;
4. no electrons or muons;

The sample contains 56 events. τ decays to hadrons are expected to give origin to a jet with low charged multiplicity (the fraction of τ decays in five or more charged is less than 1‰) and very narrow (energy is much larger than the decay Q-value). Three parameters are used to select events on the basis of the jet shape:

1. the ratio F between the energy flow in a cone of semiaperture $\Delta R = 0.4$ around the jet axis to the energy flow in a larger cone of semiaperture $\Delta R = 0.7$ (for a narrow jet F is expected to be near to 1);
2. the charged multiplicity n_c;
3. the separation $r = (\Delta\phi^2 + \Delta\phi^2)^{1/2}$ between the jet axis and the track with highest momentum.

Monte Carlo simulation gives the expected probability (P_F, P_{n_c}, P_r respectively) distribution for each variable in the τ hypothesis. For each event the τ likelihood L_τ is calculated:

$$L_\tau = \ln (P_F \cdot P_{n_c} \cdot P_r) \qquad (35)$$

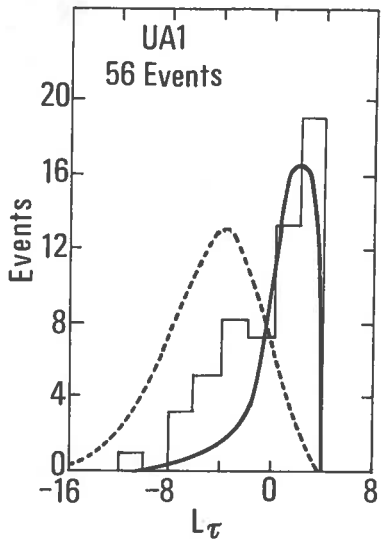

FIGURE 22

Distributions of L_τ for the data (56 events, solid histogram), the $\tau \rightarrow$ hadrons + ν Monte Carlo absolute normalized (solid curve), and UA1 jet data normalized to 56 events (dashed curve).

Fig. 22 shows the L_τ distribution for the 56 events compared with the behaviour expected for τ events and also with distribution measured for ordinary QCD jets. The τ sample is selected requiring $L_\tau > 0$ (that accepts 78% of the τ to hadrons decays) it contains 32 events.

As one can see from Fig. 22 the complementary sample $L_\tau < 0$ of 24 events[19] contains clearly non-τ events.

Are these events signaling some new phenomenon? Monte-Carlo simulation taking into account contributions from known processes and the characteristics of the experiment predicts

$W \to \tau\nu$	8.0 events
$\bar{p}p \to (Z^0 \to \nu\bar{\nu}) + \text{jet(s)}$	7.1 events
jet(s) fluctuations	3.4 events
$W \to e\nu, \mu\nu$ misidentified	2.1 events
tot.	20.8 events

a number fully compatible with the observed 24 events. Fig. 23 shows the distributions of the jet transverse energy and p_T^{mis} for the sample with $L_\tau < 0$, compared with the Monte Carlo prediction; known sources explain the data and we can put limits on new physical phenomena. This will be done in Chapter 7.

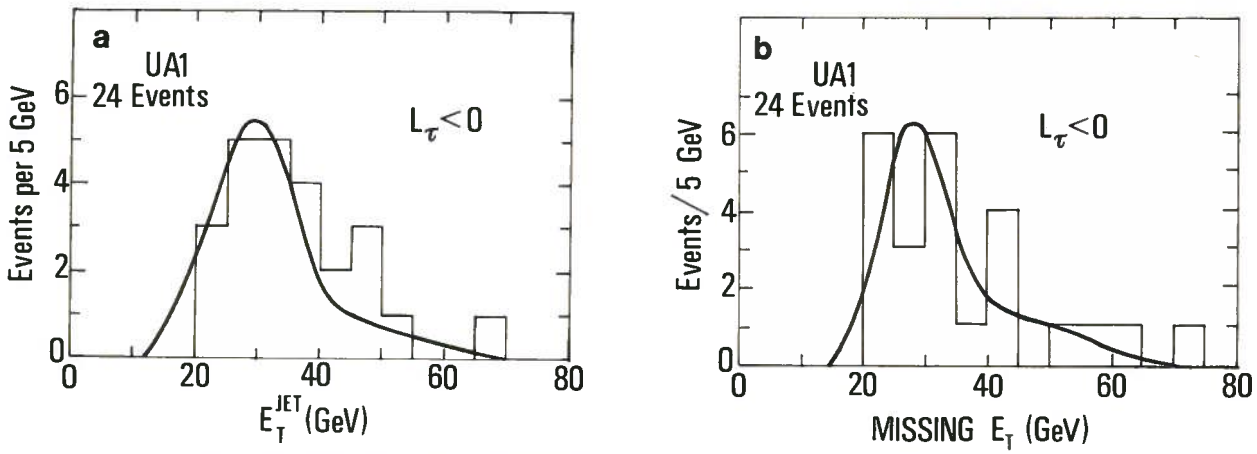

FIGURE 23

a) Jet transverse energy distribution for events passing the cut $L_\tau < 0$, (histogram) compared with all expected contributions (solid line).

b) Missing transverse energy distribution for events passing the cut $L_\tau < 0$,

The same simulation predicts for the $L_\tau > 0$ sample 28.7 ± 1.5 τ events and 2.7 ± 0.6 background events to be compared with the observed 32 events. The jet E_T and p_T^{mis} distribution are also well reproduced by the simulation as shown in Fig. 24.

The transverse mass distribution for the jet missing momentum system is shown in Fig. 25 compared with the curve for the expected value $M_W = 83.5$ GeV. A maximum likelihood fit to determine M_W gives[12]:

$$M_W = 89 \pm 3 \pm 6 \text{ GeV} \qquad (36)$$

In conclusion the W is observed also in the $\tau\nu$ final state with a value of the mass fully consistent with expectations.

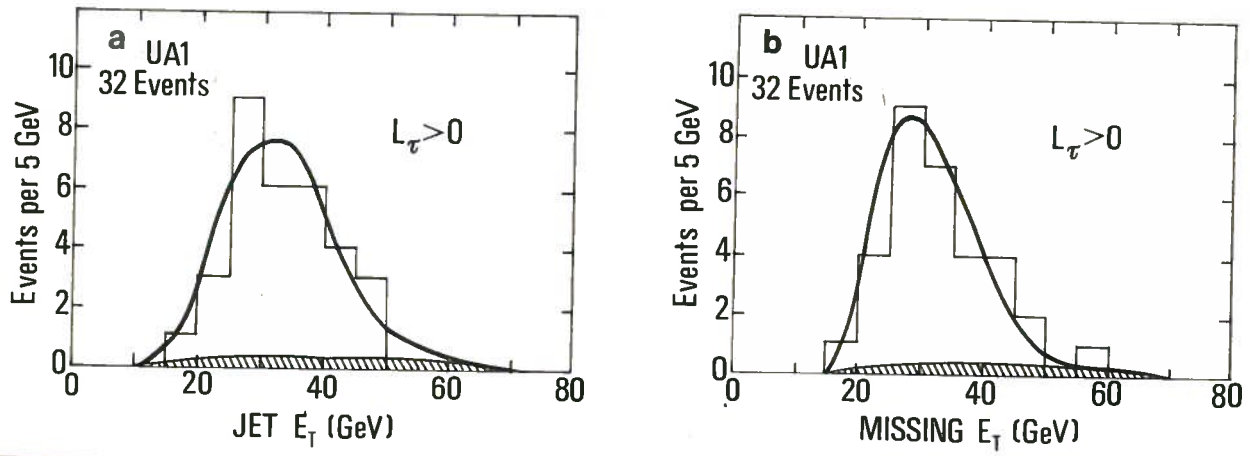

FIGURE 24

a) Jet transverse energy distribution for events passing the τ selection cut $L_\tau > 0$ b) Missing transverse energy distribution for events passing the τ selection cut $L_\tau > 0$ (histogram) compared with the prediction of the Monte Carlo for tau's from W decay (28.7 events, upper curve) and the predicted background processes (2.7 events, shaded).

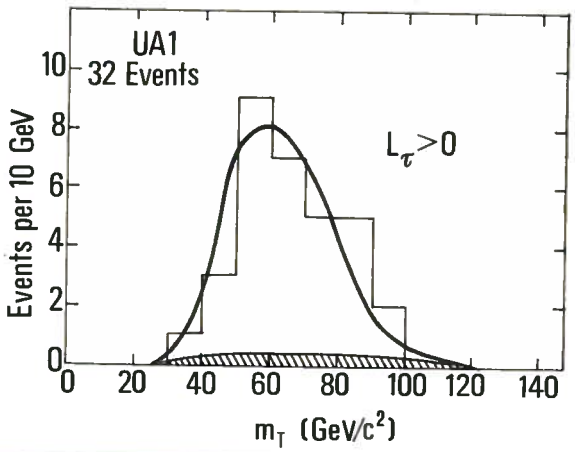

FIGURE 25

Transverse mass distribution for events passing the τ selection cut $L_\tau > 0$ (histogram) compared with the prediction of the Monte Carlo for tau's from W decay and background processes.

5. PRODUCTION PROPERTIES OF W AND Z

5.1 THE CROSS SECTIONS

The cross sections for W production followed by the decays into $e\nu$, $\mu\nu$ and $\tau\nu$ and for Z^0 production followed by the decays into $e^+ e^-$ and $\mu^+ \mu^-$ are calculated from the events in the sample discussed in the previous chapter subtracting the background contributions and correcting for detector acceptance and for selection criteria inefficiency. The total luminosity, continuously monitored during the data taking runs, is known with ±15% uncertainty that gives a corresponding systematic uncertainty on cross section values. Fig. 26 shows the measured cross sections[12] compared with the theoretical QCD predictions of Altarelli et al.[5]; the uncertainties

on these arise from the uncertainties on the structure functions, from the ambiguities on the choice of the Q^2 scale and from the not yet evaluated contribution of higher order terms. The UA2 results[21] are also in good agreement. To give the reader a feeling of the sensitivity of the theory to the input structure functions, we note that if we use the new measurement of $F_2^{\mu p}(x)$ from BCDMS[22] the predicted cross sections increase by 20% in even better agreement with the measured values.

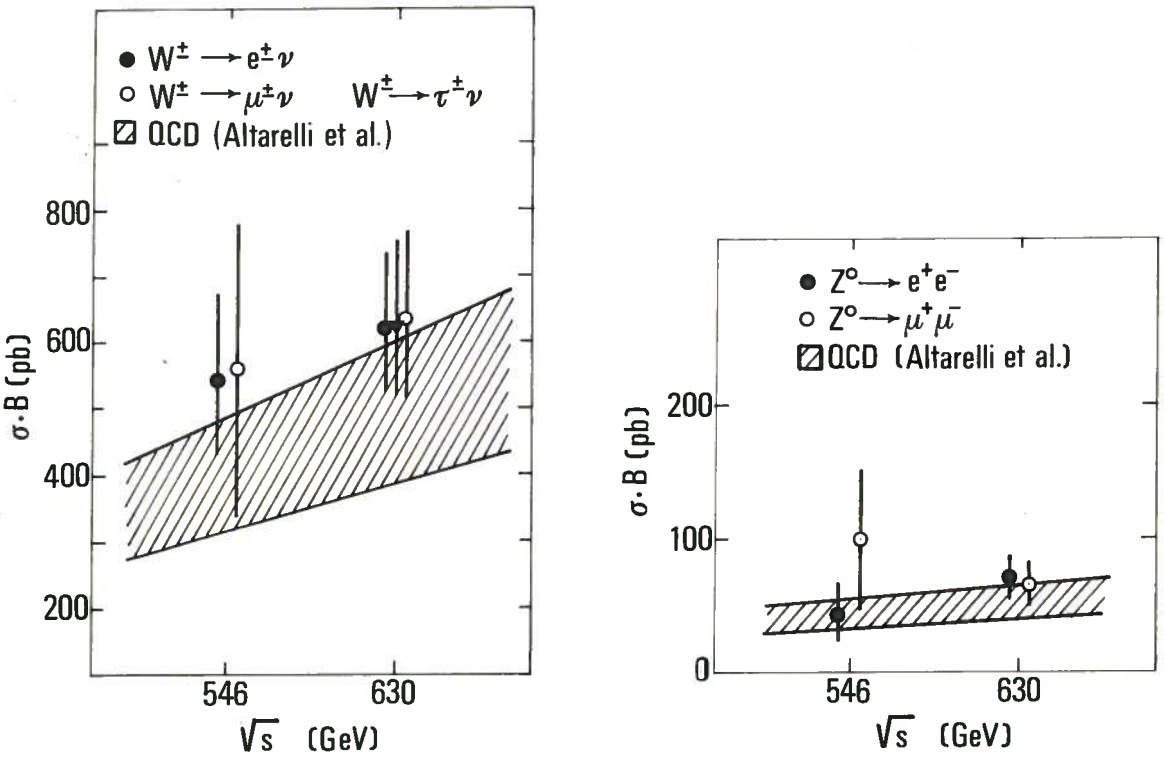

FIGURE 26
W and Z production cross sections times leptonic branching ratio as measured by UA1 compared with QCD predictions (shaded area).

5.2 *TEST OF THE UNIVERSALITY*

Independently on QCD calculations the ratio of the cross sections in the different leptonic channels gives a test of universality of the leptonic coupling at the energy scale M_W/M_Z.

The square roots of the rations of cross sections give the ratios of the coupling constants. For the charged currents (W)[20]:

$$g_\mu/g_e = 1.00 \pm 0.07\ (\text{stat}) \pm 0.04\ (\text{syst}) \qquad (37a)$$

$$g_\tau/g_e = 1.01 \pm 0.10\ (\text{stat}) \pm 0.06\ (\text{syst}) \qquad (37b)$$

and for the neutral currents (Z)[20]:

$$k_\mu/k_e = 1.02 \pm 0.15 \pm 0.04 \qquad (38)$$

The uncertainty on the luminosity obviously cancels in the ratios.

5.3 NUMBER OF COLOURS AND NUMBER OF NEUTRINO SPECIES

The theoretical calculation mentioned in Sect. 5.1 depends also on: 1) the value of the top mass (assumed to be $M_t = 40$ GeV); varying M_t the changes of the cross sections are small compared to other uncertainties; 2) the number of colours N_c; 3) the number of neutrino species N_ν. The number of colours enters in the calculation of the cross sections in two ways: the probability for a quark to meet an antiquark of the same colour in the initial state is $1/N_c$, the total widths of the IVB depend on N_c (the number of decay channels depends on N_c). We have:

$$\sigma B_{e\nu}(\bar{p}p \to W \to e\nu) = \frac{1}{N_c} \sum_{(q\bar{q})} \sigma(q\bar{q} \to W) \frac{\Gamma(W \to e\nu)}{\Gamma_W^{tot}(N_c)}$$

In a first approximation the branching ratio can be evaluated by counting the final states:

$$\frac{\Gamma(W \to e\nu)}{\Gamma_W^{tot}} \approx \frac{1}{N_L + N_c \cdot N_Q}$$

where N_L and N_Q are the numbers of lepton and quark families respectively. The correct calculation for $N_c = 2$ and $N_c = 4$ (the two cases nearer the expected $N_c = 3$ value) gives:

$$\frac{\sigma \cdot B(N_c = 2)}{\sigma \cdot B(N_c = 3)} = 1.9 \quad ; \quad \frac{\sigma \cdot B(N_c = 4)}{\sigma \cdot B(N_c = 3)} = 0.6 \qquad (39)$$

both values being inconsistent with data[20] at 90% c.l. we have a further test of QCD assumption $N_c = 3$.

Up to now we have seen that the collider data are in very good agreement with Electroweak theory and with QCD. The Standard Model does not make any prediction on the number of fermion families nor on the masses. Two important questions are open: what is the top mass and how many families are realized in Nature. We will start from the second question observing that it is equivalent to ask how many are the neutrino species, N_ν. An indirect limit exists based in the comparison of the He/H abundance ratio in the Universe and the calculations in the Big-Bang model. Two calculations give upper limits[23] $N_\nu < 4$ and $N_\nu < 6$ valid for neutrino masses not bigger than 1 MeV.

A more direct evaluation, valid for $M_\nu << M_Z/2$, can be obtained from the measurement of Γ_Z. In fact, in the assumption that charged leptons and quarks of further generations are so heavy that do not contribute to Z^0 decays, the total width of the Z^0 is:

$$\Gamma_Z = \Gamma_Z\,(3\ \text{gen}) + (N_\nu - 3)\,\Gamma_Z\,(\nu\bar{\nu}) \qquad (40)$$

where Γ_Z (3 gen) is the total width expected for 3 generations and $\Gamma_Z(\nu\bar{\nu}) = 170$ MeV is the expected contribution of each neutrino species.

Unfortunately a measurement of Γ_Z does not exist yet (it will come from LEP) but only the upper limits (18). From them we have

$$N_\nu \leq 16 \tag{41}$$

Much more sensitive limits are obtained starting from the observation that the number of $W \rightarrow l\nu$ where l means a charged lepton, and $Z^0 \rightarrow ll$ decays are sensitive to additional open channels like $Z^0 \rightarrow \nu\bar{\nu}$. As originally suggested by N. Cabibbo [24] the ratio

$$R = \frac{\sigma(W \rightarrow l\nu)}{\sigma(Z \rightarrow ll)} = \frac{\sigma_W}{\sigma_Z} \frac{BR(W \rightarrow l\nu)}{BR(Z \rightarrow ll)} \tag{42}$$

is free from many theoretical uncertainties and from the experimental uncertainty in the luminosity.

The R parameter can be written as the product of three factors:

$$R = \frac{\Gamma(W \rightarrow l\nu)}{\Gamma(Z \rightarrow ll)} \cdot \frac{\Gamma_Z}{\Gamma_W} \cdot \frac{\sigma_W}{\sigma_Z} \tag{43}$$

The first factor, the ratio of the partial leptonic widths is well known from Electroweak theory; the second factor, the ratio of the total widths, can be reliably calculated when all the different decay channels are known. Let us assume for the moment that charged leptons and quarks of possible heavier families are heavy enough that their contributions to W and Z^0 widths can be neglected and that all the neutrinos of these families are light enough that no phase space suppression takes place in the Z^0 decay ($M_\nu << M_Z/2$). Γ_W then depends only on M_t (it is a decreasing function of M_t) and Γ_Z depends essentially only on N_ν (it is an increasing function of N_ν). In principle Γ_Z depends also on M_t up to $M_t = M_Z/2$ where the $t\bar{t}$ channel closes; we can ignore this dependence, given the experimental lower limit $M_t > 44$ GeV (see Chapter 7).

The third factor in (43), the cross section ratio, is the most uncertain as its calculation is based on QCD. The main uncertainties are due to the structure functions and the Weinberg angle. The best estimate is[20]:

$$\frac{\sigma_W}{\sigma_Z} = 3.\,23 \pm 0.\,10 \tag{44}$$

The R parameter has been measured by UA1[20] and UA2 [21]:

$$\text{UA1} \qquad R = 9.\,1^{+1.\,7}_{-1.\,2} \quad ; \quad R < 11.5 \text{ (90\% c.l.)} \tag{45}$$

$$\text{UA2} \qquad R = 7.\,2^{+1.\,7}_{-1.\,2} \quad ; \quad R < 9.5 \text{ (90\% c.l.)} \tag{45}$$

The results are consistent and can be combined giving:

$$R = 8.\,4^{+\,1.\,2}_{-\,0.\,9} \quad ; \quad R < 10.1\ (90\%\ \text{c.l.}) \tag{46}$$

The upper limit on R can be translated in an upper limit, function of M_t, on Γ_Z using formula (43) hence in an upper limit (again a function of M_t) on N_ν using (40). The result is shown in Fig. 27 where $\sigma_W/\sigma_Z = 3.13$ as been taken (the less constraining value at one standard deviation from the most probable value in (44)).

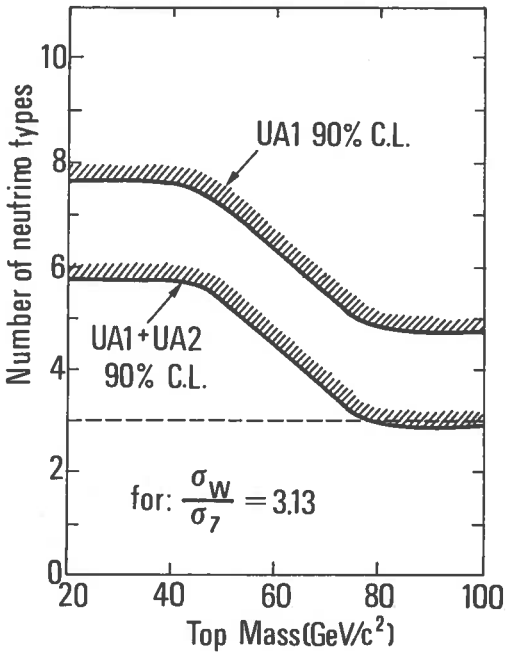

FIGURE 27
Limits (90% c.l.) from UA1 and UA1 + UA2 data on the number of neutrinos as a function of M_t.

Taking into account the above mentioned lower limit on M_t we conclude that[20]:

$N_\nu < 5.7$ at 90% c.l.

that, being N_ν necessarily integer, means:

$$N_\nu \leq 5 \tag{47}$$

The limit becomes even more stringent if M_t is bigger. In particular if $M_t > 75$ GeV the existence of a fourth neutrino flavour (a fourth generation) is highly unlikely.

If we now allow for the decay $W \to L\nu_L$, where L is the fourth generation lepton and with mass $M_L > 41$ GeV (as we will see in Sect. 7.1) the limit becomes worse by one neutrino species.

A similar method has been used to place an upper limit on N_ν at $e^+ e^-$ machines. The process $e^+e^- \to Z^0\gamma \to \nu\bar{\nu}\gamma$ (with virtual Z^0) gives origin to the peculiar final state: one γ + missing

energy. The cross section is perfectly calculable and is a function of N_ν. The upper limit obtained combining the data of the experiments ASP, MAC and CELLO[25] is $N_\nu < 4.9$ (90% c.l.). Again little space is allowed for not yet known neutrino flavours.

5.4 W TRANSVERSE MOTION

Experimentally events with a W emitted at moderate or high transverse momentum (p_T^W) are observed. In all of them p_T^W is balanced by the transverse momentum of one or (more rarely) more jets. In the QCD interpretation the production process of the W via quark-antiquark annihilation discussed in Chapter 2 is only the lowest order process; at higher orders gluon radiation from one of the initial quarks is expected giving exactly the observed topology.

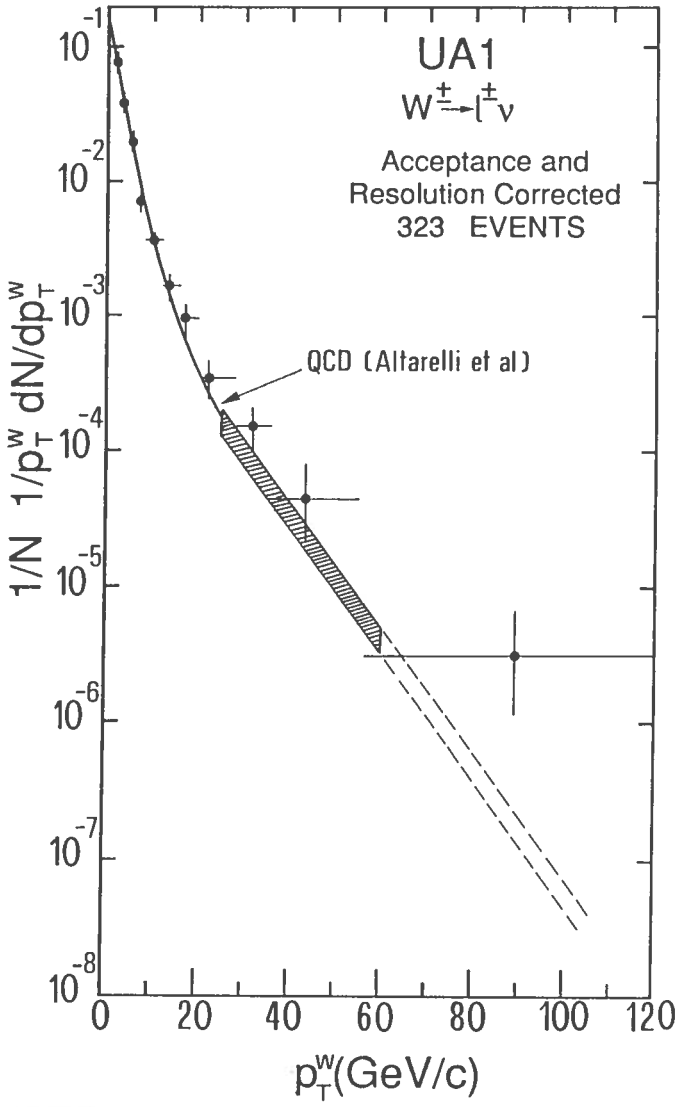

FIGURE 28

W transverse momentum distribution for both $W \to e\nu$ and $W \to \mu\nu$ events.

At sufficiently high values of p_T^W perturbative QCD calculations are feasible and in fact have been done by G. Altarelli et al.[5] and a quantitative test of the theory is possible.

Fig. 28 shows the invariant differential cross section[26] compared with the QCD calculations. Data (323 W leptonic decays) have been corrected for detection and selection efficiency and resolution. We observe very good agreement with the theory. At very high p_T^W the agreement is not perfect: for $p_T^W > 80$ GeV 0.2 ± 0.06 events are expected, 2 are observed. This is not of course an inconsistency but a closer observation shows that their topology (both events contain two jets with invariant mass near to M_W) is very unlikely in the QCD calculation. More statistics is needed to clarify this point, **the only found where the agreement with the S.M. is not perfect.**

6. THE SEARCH FOR TOP

The only not yet observed quark of the three known families is the top quark. Its existence is required to cancel flavour-changing neutral currents as necessary, in the specific case, to explain the experimental upper limit for the branching ratio of the B^0 into $\mu^+ \mu^-$ anything of 10^{-3}. The theory des not give any prediction for M_t, but the theoretical upper limit $M_t < 180$ GeV can be obtained, as shown in Sect. 4.3.

An experimental lower limit, $M_t > 25$ GeV, comes from the non observation of top at the highest energy $e^+ e^-$ collider, TRISTAN[27].

At a $p\bar{p}$ collider two processes are expected to give rise to top[28]: through W decay into $t\bar{b}$ (or $\bar{t}b$) and through direct strong (QCD) production of $t\bar{t}$. To have a not too unfavourable signal to background ratio, semileptonic decays of the t:

$$t \to \mu b \nu \qquad \text{or} \qquad t \to e b \nu$$

that are expected to have branching ratios of ~1/9, must be considered. In both cases the expected topology is: one high p_T lepton (μ or e), two hadronic jets (one for $\bar{b}$ produced with t, one for b of the decay of the t) and p_T^{mis}. Fig. 29 shows, on the left scale, the expected number of events (before any selection cut).

The principal physical background is due to the processes:

$$\begin{array}{lllll} p\bar{p} \to b\bar{b}g & ; \quad b \to \mu \nu c & ; \quad \bar{b} \to \text{jet} & ; \quad g \to \text{jet} & \\ \bar{p}p \to c\bar{c}g & ; \quad c \to \mu \nu s & ; \quad \bar{c} \to \text{jet} & ; \quad g \to \text{jet} & (48) \end{array}$$

Fig. 30 shows that the signal is expected to be one order of magnitude less than the background. It is then necessary to apply selection criteria to enhance the relative top contribution. We must also observe that p_T^{mis} is in this case much smaller than for $W \to l\nu$ (its value is in fact of the same order of the experimental resolution) and that p_T^l is of the order of 10 - 20 GeV, a region where the identification of both electron and muon is difficult; accurate control of both the instrumental and the physical backgrounds is mandatory. Note also that the topology under study

contains jets and that the lepton from the t decay is often not far from the b jet; we will then start considering the μ channel that is experimentally cleaner.

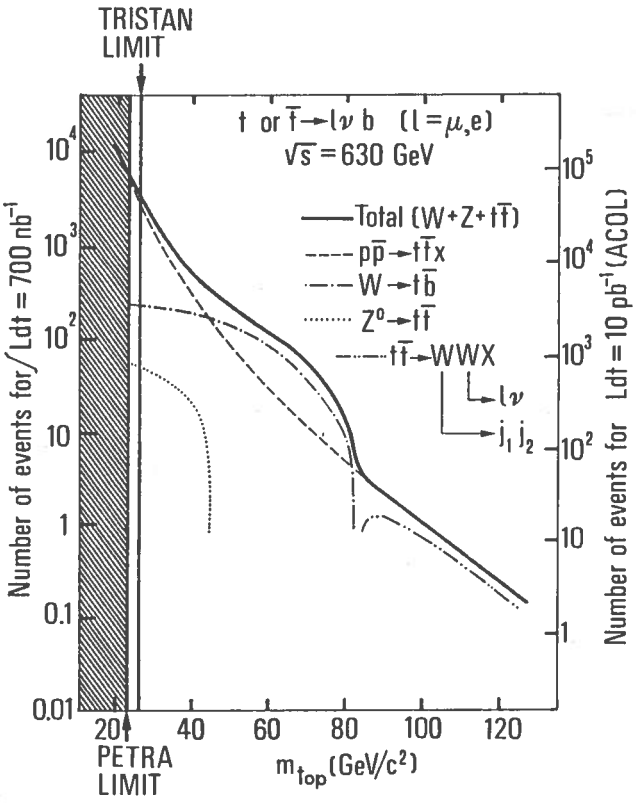

FIGURE 29
Expected numbers of events from top semileptonic decay as functions of M_t.

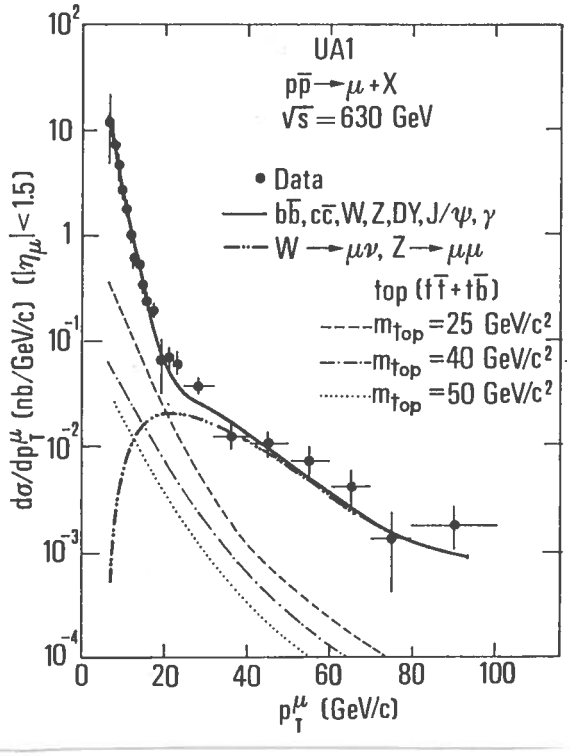

FIGURE 30
Inclusive μ production cross section and expected top contribution.

The t decay into μ b ν is much more "esothermic" than the muonic decay of the b or the c (due to the high value of M_t). As a consequence μ's from t are much more isolated than those from the background (48). The isolation variable is then of great importance to enhance signal to background ratio.

Simulation calculations have been done to evaluate the expected contributions of the physical and instrumental backgrounds. Their results have been checked on a sample of events selected to consist essentially of background. The selection criteria (one μ and two jets, $10 < p_T^\mu < 15$ GeV, transverse energy of the highest energy jet bigger than 12 GeV) provide 858 events. The Monte Carlo calculations include contributions from known processes and predict 380 ± 5 events from processes (48), 235 ± 22 events from π and K decays, 24 ± 1.5 events from W, Z, J/ψ etc. for a total of expected 639 ± 23 events in reasonable agreement with the observations. More important, the distributions of all the relevant kinematical variables have been checked and agreement between data and simulation always observed, showing that the background is fully understood.

Let us now define an isolation variable I that takes into account both the C.D. measurements (p_T) and the calorimeter measurements (E_T)

$$I=\left[\left(\sum E_T/3\right)^2+\left(\sum p_T/2\right)^2\right]^{1/2}$$

in a cone of $\Delta R = 0.7$. The study of this variable allows the optimization of the selection criteria.

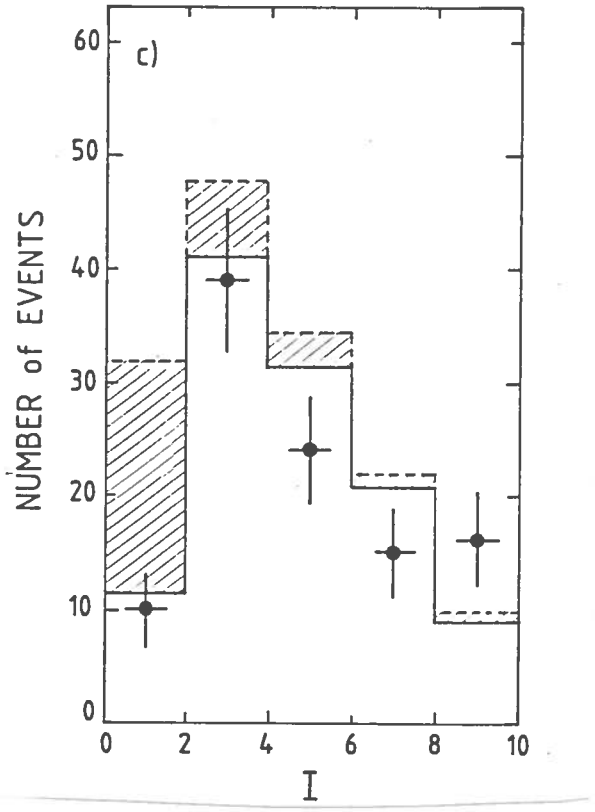

FIGURE 31
Isolation distribution for the sample described in the text. Histogram gives the predictions not including top. Shaded area gives the expected contribution for top with $M_t = 30$ GeV.

Fig. 31 shows the distribution of I for the sample with at least two jets, $p_T^{\mu} > 12$ GeV, E_T of the highest energy jet > 12 GeV and transverse invariant mass $M_T(\mu\nu) < 40$ GeV. The histogram is the result of the simulation and is seen to account perfectly for the data.

As the data do not require any top contribution and as the top production is a decreasing function of M_t we can put a lower limit on M_t. Again with a Monte Carlo calculation we evaluate the expected contribution of the two top channels for different values of M_t. The results for $M_t = 30$ GeV is shown hatched in Fig. 31. It is clear that this value is not compatible with the data. Fig. 32 shows the experimental upper limits on t the $t\bar{t}$ and $t\bar{b}$ cross sections compared with the expected values as functions of M_t. The crossing points give the lower limits (at 90% and 95% c.l.) for M_t. We note that the contribution to top production of W decays is estimated with high reliability (and is shown dashed in Fig. 32), on the contrary the QCD calculation for $t\bar{t}$ production is uncertain probably by a ±50%. This problem is illustrated in Fig. 33, where the ratios between various QCD cross section calculations (with different choices of structure functions and Q^2 scale) and a particular one (σ_0) are reported as a function of M_t. The

experimental upper limit curve (95% c.l.) is obtained from the complete information of the muon and electron (not discussed here) channels. The most pessimistic limit[22] is obtained from the lowest theoretical prediction:

$$M_t > 44 \text{ GeV} \qquad (95\% \text{ c.l.}) \tag{49}$$

This limit puts the top search out of the reach of LEPI and SLC. The increase in statistic expected with ACOL and upgrade of UA1 and UA2 will allow both experiments to push the limit up to 70 GeV or, hopefully, to discover the top.

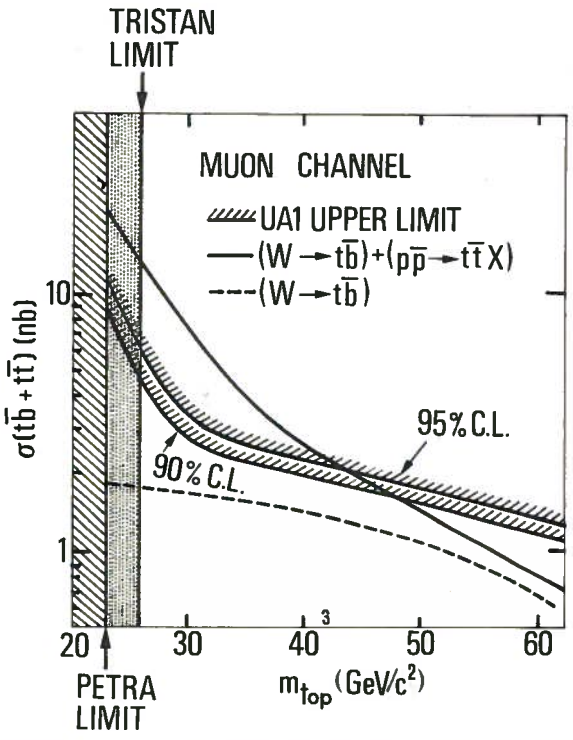

FIGURE 32
Confidence level contours in the top cross section versus M_t plane from μ channel. Solid curve refers to Monte Carlo (EUROJET) calculation.

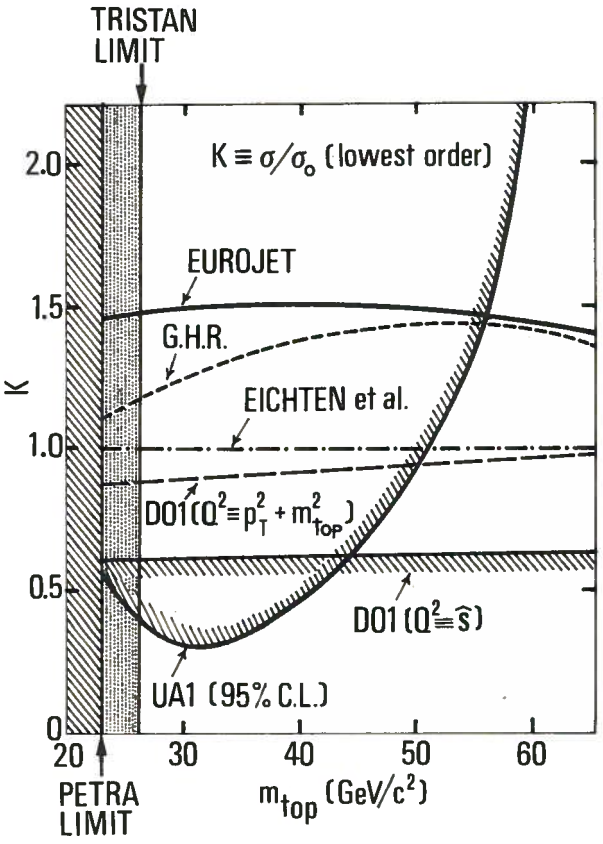

FIGURE 33
Sensitivity of the mass limit to the ratio $K = \sigma(t\bar{t})/\sigma_0$ where σ_0 is the lowest order cross section calculation using EHLQI structure functions and $Q^2 = M_t^2 + p_T^2(K = 1)$. The choice of structure function D01, $Q^2 = \hat{s}$ gives the lowest cross section.

7. SEARCH FOR EXTENSIONS AND MODIFICATIONS OF THE STANDARD MODEL

7.1 SEARCH FOR HEAVY LEPTON

As mentioned before the Standard Model does not specify the number of quark and lepton families. Direct searches of the fourth generation charged lepton L in $e^+ e^-$ collisions have placed a lower limit on its mass $M_L > 22.7$ GeV (90% c.l.). At the $\bar{p}p$ collider the heavy lepton is expected to be present in the W decay $W \to L\nu_L$ (with universal coupling), giving a contribution to the high

E_T^{mis} sample (when the L decays semihadronically). As discussed in Sect. 4.5 no such contribution is necessary as the data are completely explained by standard sources. As the number of events expected from the heavy lepton is a decreasing function of its mass, we can put a lower limit on M_L.

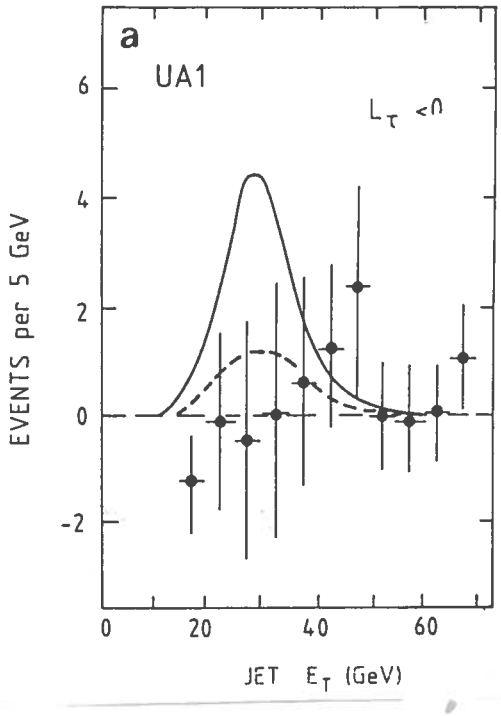

FIGURE 34
Jet transverse energy distribution for background-subtracted $L_\tau < 0$ events. Solid line is the expected contribution of heavy lepton with M_L = 35 GeV, dashed line for M_L = 55 GeV.

The heavy lepton contribution was evaluated with a Monte Carlo calculation with full detector simulation, including trigger and selection criteria acceptance[19]. The simulation shows that the process populates preferentially the region $L_t < 0$, E_T (jet) < 40 GeV that is then considered for the analysis. In this region we expect 16 events for M_L = 25 GeV, 7.6 events for M_L = 45 GeV and 1.4 events for M_L = 65 GeV. The additional contributions to the E_T (jet) distribution, after subtraction of standard sources, is shown in Fig. 34 for M_L = 35 GeV and M_L = 55 GeV. Taking into account the contribution of Z^0 + jet followed by $Z_0 \rightarrow \nu_L \bar{\nu}_L$ we derive the limit [19]

$$M_L > 41 \text{ GeV} \qquad (90\% \text{ c.l.}) \tag{50}$$

The upgraded experiments UA1 and UA2 with the increased luminosity of ACOL are expected to move the limit to about 70 GeV where the channel $W \rightarrow L\nu_L$ starts closing.

7.2 SEARCH FOR SUPERSYMMETRIC PARTICLES

Theoretical speculations predict the existence for each known particle of a supersymmetric partner. In many models the lightest supersymmetric particle, the photino $(\tilde{\gamma})$, is stable and behaves much like a neutrino, non interacting with matter. "SUSY" particles are as a consequence

expected in final states with large missing p_T. Again the non observation of any unexpected contribution in the large p_T^{mis} sample allows us to put limits on the SUSY particles masses. (SUSY theory gives no prediction for the masses but specifies the coupling constants).

Given the richness of the hypothesized supersymmetric zoo a specific model must be used. We will assume that the 5 lower mass squarks $(\tilde{q})$ have the same mass $M_{\tilde{q}}$ and no contribution from $\tilde{H}$, $\tilde{Z}$, $\tilde{W}$, $\tilde{t}$. We will also assume the photino to be massless and we will consider the strong production of **squarks** and **gluinos** $(\tilde{g})$ through the following processes:

$$\bar{p}p \rightarrow \tilde{g}\tilde{g} + \text{ anything}$$
$$\rightarrow \tilde{q}\bar{\tilde{q}} + \text{ anything}$$
$$\rightarrow \tilde{g}\tilde{q}(\tilde{g}\bar{\tilde{q}}) + \text{ anything}$$

that have cross sections calculable by QCD for given values of $M_{\tilde{g}}$ and $M_{\tilde{q}}$. Gluinos and squarks are not stable; in the case $M_{\tilde{q}} > M_{\tilde{g}}$, the decays are $\tilde{q} \rightarrow q\tilde{g}$, $\tilde{g} \rightarrow q\bar{q}\tilde{\gamma}$, in the case $M_{\tilde{q}} < M_{\tilde{g}}$ the decays are $\tilde{q} \rightarrow q\tilde{\gamma}$, $\tilde{g} \rightarrow \bar{q}\tilde{q}$ or $q\bar{\tilde{q}}$. In both cases the event topology consists on a number of hadronic jets from fragmentation of quarks and on p_T^{mis} from the $\tilde{\gamma}$.

Fig. 35 shows the bounds[30] obtained in the plane $M_{\tilde{q}}$, $M_{\tilde{g}}$ for $M_{\tilde{q}} >> M_{\tilde{g}}$ the bound is $M_{\tilde{g}} > 53$ GeV, for $M_{\tilde{g}} >> M_{\tilde{q}}$, $M_{\tilde{q}} > 45$ GeV.

These limits are expected to be moved to about 100 GeV with the increased luminosity of ACOL and to 200 GeV at the Tevatron. This shows the importance of the available energy.

Supersymmetric leptons, if light enough, should be produced by W (and Z^0) decays. In particular the scalar electron $\tilde{e}$ should be observed in the decay:

$$W \rightarrow \tilde{e}\,\tilde{\nu}$$
$$\quad\;\; \downarrow \rightarrow e\tilde{\gamma}$$

This process is completely calculable, for given values of the masses, because the couplings are predicted by the theory. Its topology is similar to the standard $W \rightarrow e\nu$ decay with a high p_T isolated electron and opposite p_T^{mis} (from the $\tilde{\nu}$ and $\tilde{\gamma}$). The difference is in the p_T^e distribution (no Jacobian peak) and in the ϑ^* distribution (substantially no asymmetry). As these distributions are found in perfect agreement with the standard theory the lower limits shown in Fig. 36 can be placed on the masses $M_{\tilde{\nu}}$ and $M_{\tilde{e}}$[13].

As a final observation we remind the reader that some theories postulate the existence of further IVB's analogous of W and Z at higher masses. No such event having been observed the following limits on the masses can be placed:

$$M_{W'} \geq 232 \text{ GeV} \quad ; \quad M_{Z'} \geq 188 \text{ GeV} \quad \text{at 90\% c.l.} \qquad (51)$$

if W' and Z' have the same coupling of W and Z.

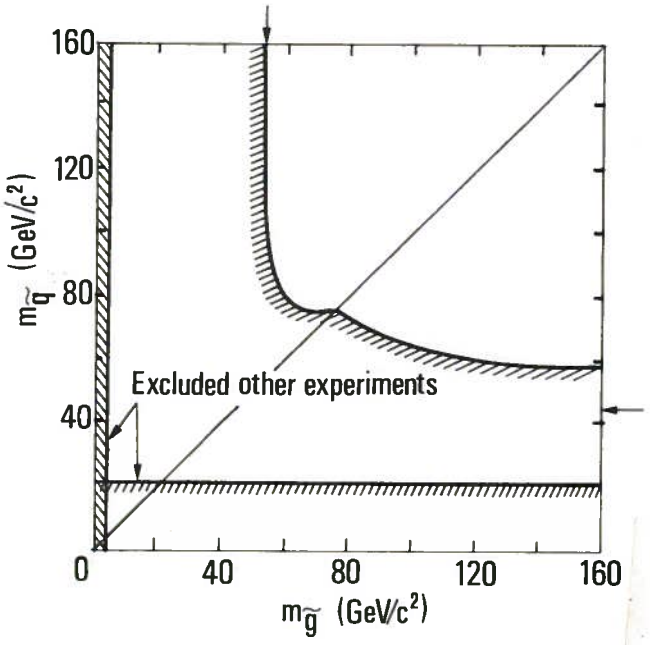

FIGURE 35
Limits (at 90% c.l.) on squark and gluino masses. The arrows indicate the asymptotic values of the 90% c.l. contour as the squark or gluino mass becomes infinitely large.

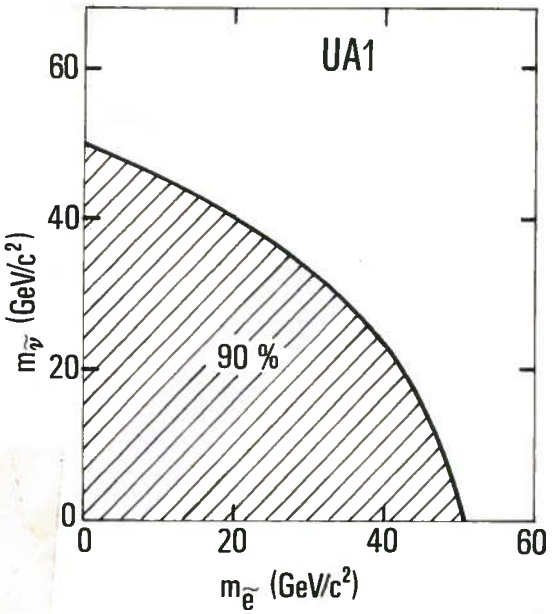

FIGURE 36
Limits (90% c.l.) on scalar electron and scalar neutrino masses.

8. LIMITS ON THE DIAMETER OF QUARKS

One of the very first observations of UA1 and UA2 was the clear evidence of jets in the high E_T events, where E_T is the scalar sum of the transverse energies of the particles emerging from the collision. In practice all the events with E_T larger than, say, 20 GeV contain jets. The great majority of the events contains two, opposite in azimuth jets; in about 10% of the cases a third jet is present, more rarely a fourth one.

We obviously interpret these events as due to hard scattering of two partons $(q, \bar{q}, g)$ that then fragment in the final state in jets, occasionally gluon radiation gives origin to a further detectable jet. The spectators give also origin to jets, but at low p_T. The situation is depicted in Fig. 37; Fig. 8 gives an examples of a two-jet event.

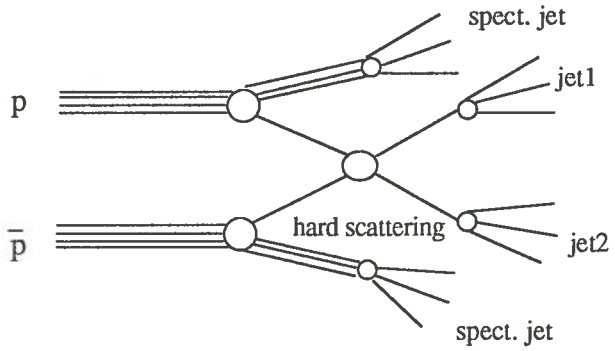

FIGURE 37

The jet identification is relatively easy at high p_T at collider energies. The following step is the identification of the energy and direction of the jet with those of the parton that has originated it. This involves systematic distortions that are calculated through Monte Carlo calculations. The procedure leaves of course uncertainties of both theoretical and experimental nature. Not withstanding these limitations jet physics is extremely interesting being a window on the elementary interactions at the parton level. Jet physics will not be discussed in these lectures, we will only mention one important result that provides a lower limit on the diameter of the quark.

If quarks are composite objects, they are expected to have a non zero diameter. The interaction between their constituents will be mediated by some mediator of high mass and will reduce to a contact term g^2/Λ_c at low energy. The diameter of the quark in this hypothesis is $1/\Lambda_c$.

From elementary optics it is well known that to resolve structures of diameter D the wavelength of the "light" should be $\lambda \leq 2D$. The resolving power achievable with a beam of momentum $p = 2\pi/\lambda$ is then $D_{min} = \pi/p$.

In the scattering of partons $p \approx \sqrt{\hat{s}}/2$ and, typically, $\sqrt{\hat{s}} = (1/6)\sqrt{s}$. At $\bar{p}p$ energy $\sqrt{s}$ the minimum observable substructure diameter is then:

$$D_{min} \approx \pi / p = 2\pi / \sqrt{\hat{s}} \approx 1 / \sqrt{s}$$

We can select a sample of events dominated by the process[31]:

$$q\bar{q} \rightarrow q\bar{q} \rightarrow \text{jet} + \text{jet}$$

taking events with only two high E_T jets and with high invariant dijet mass, M_{jj}. In this way partons carrying a great fraction of the proton (or antiproton) momentum are selected, that are dominantly (valence) quarks and not gluons. The directions of the jets are well measured and are expected to be very near to the partons directions (the same is not true for the energies). We can then reliably measure the quark-quark scattering differential cross section. In a first approximation for point like quarks this is expected to be the Rutherford cross section:

$$d\sigma / d\cos\vartheta \cong \frac{\alpha_s^2}{\hat{s}}(1 - \cos\vartheta)^{-2} \qquad (52)$$

Any quark structure is expected to show up as an increased counting rate at large angles. This is exactly the same experiment as done on atoms as targets by Geiger and Marsden in 1909[32]. Before proceeding we define the useful variable:

$$\chi = (1 + \cos\vartheta) / (1 - \cos\vartheta) \qquad (53)$$

that has a constant distribution for Rutherford scattering. Fig. 38 shows the measured $d\sigma/d\chi$ for dijet events with $240 < M_{jj} < 300$ GeV.

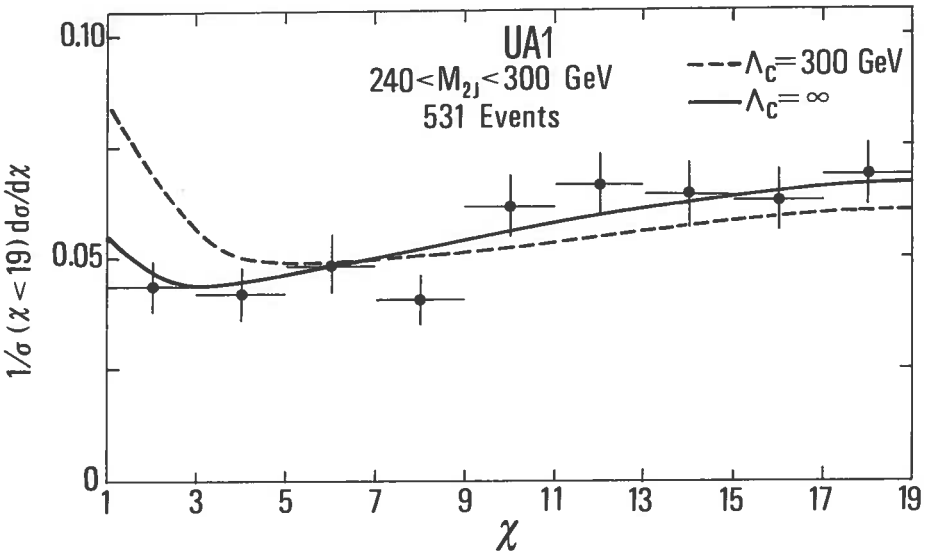

FIGURE 38

The angular distribution $(1/\sigma)\,(d\sigma/d\chi)$ for the very high mass ($240 < m_{2j} < 300$ GeV) jet pairs shown as a function of χ, where $\chi = (1 + \cos\theta)$ and θ is the subprocess CM scattering angle. The solid curve represents the QCD prediction which corresponds to $\Lambda_c = \infty$, and is the best fit to the data. The dotted curve, which corresponds to $\Lambda_c = 300$ GeV, is clearly excluded by the data.

The continuous line gives the behaviour expected from QCD (that is similar but not exactly equal to Rutherford) and the expectations including and additional contact term with $\Lambda_c = 300$ GeV, clearly excluded by the data. On this basis the limit is:

$$\Lambda_c > 415 \text{ GeV} \quad (95\% \text{ c.l.}) \tag{54}$$

corresponding to a quark diameter:

$$D_q < 0.5 \text{ am} \qquad (1 \text{ am} = 10^{-18} \text{ m}) \tag{55}$$

These are the most stringent limits on quarks dimensions. To have better limits **higher centre of mass energies** are needed. A limit $\Lambda_c > 2$ TeV ($D_q < 0.1$ am) is expected from Tevatron.

9. CONCLUSIONS

UA1 and UA2 working at the CERN $\bar{p}p$ collider have definitively shown that **precision physics** can be done with a hadronic collider.

The **standard model** has been verified in the force **mediators** (vector) **sector**. The spinor sector (J = 1/2) is also O.K. but we **still miss the top quark ($M_t > 44$ GeV)**. The not yet discovered families cannot be many as indicated by independent limits: $N_\nu \leq 5$ or less if top is heavy, $M_L > 41$ **GeV**, mass splitting of the quark doublet increasing going to heavier families and on the other hand near to the limits allowed by the agreement between M_W and $\text{sen}^2\vartheta_W$ for the third family.

Physics beyond the Standard Model has been searched for but no evidence for has been found. In particular limits on the masses of SUSY particles of the order of $M_Z/2$ have been established. No evidence of quark structure down to 0.5×10^{-18} m has been found.

In the next few years the upgraded UA1 and UA2 experiments are expected to collect 10 pb^{-1} integrated luminosity, an increase more than 1 fold with respect to the present samples. The upgraded calorimetry will allow a precise measurement of M_W/M_Z, while M_Z will be precisely measured at LEP. More tight tests of the Standard Model will be done.

The top quark will also be discovered if it is lighter than 70 GeV. The limits for new phenomena will be pushed to higher energy but, in this particular sector, the higher centre of mass energy of the Tevatron collider will be winning.

The scalar sector (Higgs) is on the other hand probably outside the reach of the existing hadron colliders.

Other reviews of collider results are listed in ref. 33.

REFERENCES

1. C. Albajar et al., Phys. Lett. B186 (1987) 247.

2. Particle Data Group, Phys. Lett. 170B (1986) 1.

3. A. Sirlin, Phys. Rev. D22 (1980) 971.
   W.J. Marciano, Phys, Rev., D20 (1979) 274.
   W.J. Marciano and A. Sirlin, Phys. Rev. D29 (1984) 945 and D22 (1980) 2695.
   F. Antonelli et al., Phys. Lett. 91B (1980) 90.
   M. Veltman, Phys. Lett. 91B (1980) 95.

4. H. Abramowicz et al., Phys. Lett. 57 (1986) 298.
   F. Bergsma et al., CERN-EP/87-140 (1987). To be published in Z. Phys. C.

5. G. Altarelli et al., Nucl. Phys. B246 (1984) 12 and Z Phys. C27 (1985) 617.

6. R. Ansari et al., Phys. Lett. 168B (1987) 452

7. M. Barranco Luque et al., Nucl. Inst. and Meth. 176 (1980) 175.
   M. Calvetti et al., Nucl. Inst. and Meth. 174 (1980) 285.
   M. Calvetti et al. IEEE Trans. Nucl. Sci. NS-30 (1983) 71.

8. C. Cochet et al., Nucl. Inst. and Meth. A243 (1986) 45.
   B. Andortet et al., Nucl. Inst. and Meth. 176 (1980) 115.
   C. Bacci et al., Nucl. Inst. and Meth. 200 (1982) 195.

9. M. Corden et al., Nucl. Inst. and Meth. A238 (1985) 273.

10. G. Bauer et al., Nucl Inst. and Meth. A253 (1987) 179.
    A. Bettini et al., Nucl Inst. and Meth. A253 (1987) 189.
    G. Bauer et al., Nucl Inst. and Meth. A260 (1987) 101.

11. K. Eggert et al., Nucl Inst. and Meth. 176 (1980) 223.

12. C. Albajar et al., Phys. Lett. 185 (1987) 233.

13. G. Arnison et al., Nuovo Cimento Lett. 44 (1985) 1.
    G. Arnison et al., Europh. Lett. 1 (1986) 327.

G. Arnison et al., Phys. Lett. 166B (1986) 484.

14. UA1 Collaboration, CERN-EP/87-154 (1987).

15. R. Ansari et al., Phys. Lett. 186B (1987) 440.
R. Ansari et al., Erratum Phys. Lett. 190B (1987) 238.

16. U. Amaldi et al., Phys. Rev. D36 (1987) 1385.

17. M. Jacob, Nuovo Cimento Lett. 9 (1978) 826.

18. G. Arnison et al., Phys. Lett. 134B (1984) 469.

19. C. Albajar et al., Phys. Lett. 185B (1987) 241.

20. C. Albajar et al., Phys. Lett. 198B (1987) 271.

21. R. Ansari et al., Phys. Lett. 194B (1987) 158.

22. R. Voss, Rapporteur talk on Charged Lepton Interactions at 1987 International Symp. on Lepton and Photon Inter. at High Energies (Hamburg, July 1987) p. 1.

23. G. Steigman et al., Nature 300 (1981) 142.
J. Ellis et al., Phys. Lett. 167B (1986) 457.

24. N. Cabibbo, "What Next ?" Third Topical Workshop on Proton-Antiproton Collisions held at Rome, Jan. 1983. Proceedings CERN 83-04 (1983) 567.

25. For a review see M. Davier: "Search for New Particles", Proceedings of the XXIII Int. Conf. on HEP, Bekely 1986, p. 25.

26. C. Albajar et al., Phys. Lett. 193B (1987) 389.

27. K. Amako et al.: "New Result from VENUS";
A. Miyamoto et al.: "New Results from TOPAZ";
Y. Sakai et al.: "New Results from AMY".
Presented at " Physics in Collision VII" Tzukuba 1987.

28. C. Albajar et al. "Study of Heavy Flavour Production in Events with a Muon Accompanied by Jet(s) at the CERN Proton-Antiproton Collider", CERN-EP/87-18 and "Search for New Heavy Quarks at the CERN Proton-Antiproton Collider", CERN-EP/87-190. To be published on Z. Phys. C.

29. S. Komamiya in Proc. 1985 Intern. Symp. on Lepton and Photon Interactions at High Energies (Kjoto 1985).

30. C. Albajar et al., Phys. Lett. 198B (1987) 261.

31. G. Arnison et al., Phys. Lett. 177B (1986) 244.

32. Geiger and Mardsen. Proc. Roy. Soc. 82 (1909) 495.

33. C. Rubbia, Rev. Mod. Phys. 57 (1985) 699 (Nobel Lecture).
Lectures at the Cargese Summer School 1987 by L. Di Lella, Proton-Antiproton Collider Physics: Experimental Aspects. CERN-EP/88/02 (1988) and by M. Jacob, " $p\bar{p}$ Collider Physics, present and prospects", CERN-TN-4813 (1987).
T. Müller, Produiction Properties of Intermediate Vector Bosons W and Z at the CERN $p\bar{p}$ Collider, CERN-EP/88-48 (1988).